Walking signals in $N_f = 8$ QCD on the lattice

Yasumichi Aoki,[1] Tatsumi Aoyama,[1] Masafumi Kurachi,[1] Toshihide Maskawa,[1] Kei-ichi Nagai,[1] Hiroshi Ohki,[1] Akihiro Shibata,[2] Koichi Yamawaki,[1] and Takeshi Yamazaki[1]

(LatKMI Collaboration)

[1]*Kobayashi-Maskawa Institute for the Origin of Particles and the Universe, Nagoya University, Nagoya 464-8602, Japan*
[2]*Computing Research Center, High Energy Accelerator Research Organization (KEK), Tsukuba 305-0801, Japan*
(Received 27 February 2013; published 20 May 2013)

We investigate chiral and conformal properties of the lattice QCD with eight flavors ($N_f = 8$) through meson spectrum using the highly improved staggered quark (HISQ) action. We also compare our results with those of $N_f = 12$ and $N_f = 4$ which we study on the same systematics. We find that the decay constant F_π of the pseudoscalar meson "pion" π is nonzero, with its mass M_π consistent with zero, both in the chiral limit extrapolation of the chiral perturbation theory. We also measure other quantities which we find are in accord with the π data results: The ρ meson mass is consistent with nonzero in the chiral limit, and so is the chiral condensate, with its value neatly coinciding with that from the Gell-Mann-Oakes-Renner relation in the chiral limit. Thus, our data for the $N_f = 8$ QCD are consistent with the spontaneously broken chiral symmetry. Remarkably enough, while the $N_f = 8$ data near the chiral limit are well described by the chiral perturbation theory, those for the relatively large fermion bare mass m_f away from the chiral limit actually exhibit a finite-size hyperscaling relation, suggesting a large anomalous dimension $\gamma_m \sim 1$. This implies that there exists a remnant of the infrared conformality, and suggests that a typical technicolor ("one-family model") as modeled by the $N_f = 8$ QCD can be a walking technicolor theory having an approximate scale invariance with large anomalous dimension $\gamma_m \sim 1$.

I. INTRODUCTION

The origin of mass is the most urgent issue of the particle physics today. Although the LHC has discovered a 125 GeV boson roughly consistent with the standard model (SM) Higgs boson, there still remain many unsolved problems with the SM, which would require physics beyond the SM. One of the candidates for the theory beyond the SM towards that problem is the walking technicolor (WTC) [1] having a large anomalous dimension $\gamma_m \simeq 1$ and approximate scale invariance due to the almost nonrunning ("walking") coupling [2], which is based on the scale-invariant gauge dynamics [ladder Schwinger-Dyson (SD) equation [3,4]]. Actually, WTC predicts [1,5] a light scalar Higgs-like composite, technidilaton, a pseudo-Nambu-Goldstone boson of the spontaneously broken approximate scale symmetry, which may be identified with the 125 GeV boson [6].

The walking behavior can in fact be realized in the "large N_f QCD," QCD with large number of (massless) flavors N_f, which possesses the Caswell-Banks-Zaks (CBZ) infrared fixed point (IRFP) [7], $\alpha_* = \alpha_*(N_c, N_f) \times (<\infty)$ of the two-loop beta function, for $N_f^*(\simeq 8) < N_f < N_f^{(AF)} = 11N_c/2(= 16.5)$ in such a way that $\alpha_* \to 0$ as $N_f \to N_f^{(AF)}$, where $N_f^{(AF)}$ is the maximum number to keep the asymptotic freedom. Because of the CBZ IRFP there exists an approximate scale invariance $\alpha(\mu) \simeq \alpha_*$ in

the infrared region $0 < \mu < \Lambda_{QCD}$ ("infrared conformality"), while such a scale symmetry is lost for the ultraviolet region $\mu > \Lambda_{QCD}$ where the coupling runs as in a usual asymptotically free theory.[1] When N_f is near N_f^* so that α_* is strong enough to trigger the spontaneous chiral symmetry breaking (SχSB), the exact IRFP would actually be washed out by the dynamical generation of a quark mass $m_D \neq 0$ through a continuous phase transition ("conformal phase transition" [9]), $m_D = 0$ ($\alpha_* < \alpha_{cr}$, or $N_f > N_f^{cr}(>N_f^*)$) to $m_D \neq 0$ ($\alpha_* > \alpha_{cr}$, or $(N_f^*<)N_f < N_f^{cr}$), in such a way ("Miransky scaling" [4]) that $m_D \sim \Lambda_{QCD} \cdot \exp(-\pi/\sqrt{\alpha_* - \alpha^{cr}}) \ll \Lambda_{QCD}$ for $\alpha_* \simeq \alpha_{cr}$ ($N_f \simeq N_f^{cr}$), where α_{cr} is the critical coupling for the SχSB and N_f^{cr} the critical number of flavors such that $\alpha_*(N_c, N_f^{cr}) = \alpha_{cr}$. The critical number N_f^{cr} was estimated as $N_f^{cr} \simeq 4N_c \simeq 12$ [8] by comparing the two-loop value of the CBZ IRFP with the critical coupling of the ladder SD equation analysis [3]: $\alpha_*(N_c, N_f^{cr}) = \alpha_{cr}(= \pi/(3C_2) = \pi/4)$. Now, for $N_f(<N_f^{cr})$ very close to N_f^{cr}, the dynamical mass $m_D(\neq 0)$ could be much smaller than the intrinsic scale $m_D \ll \Lambda_{QCD}$, in

---

[1]The intrinsic scale Λ_{QCD} at two-loop level is defined as usual by a renormalization-group-invariant scale parameter $\Lambda_{QCD} = \mu \cdot \exp(-\int^{\alpha(\mu)} \frac{d\alpha}{\beta(\alpha)})$ such that $\frac{d\Lambda_{QCD}}{d\mu} = 0$, where $\beta(\alpha) \equiv \partial\alpha/\partial(\ln\mu)$ is the two-loop beta function instead of the one-loop one [8].

sharp contrast to the usual QCD where $m_D = \mathcal{O}(\Lambda_{QCD})$, so that the approximate conformality $\alpha(\mu) \simeq \alpha_*$ still remains in the wide infrared region $m_D < \mu < \Lambda_{QCD}$ as an impact of the would-be IRFP. Such a "remnant of conformality" should appear in low energy quantities. This is the case for the WTC, with the intrinsic scale Λ_{QCD} being identified with the "ultraviolet" cutoff Λ of the WTC usually taken as the extended technicolor (ETC) scale Λ_{ETC}, and will be the focus of our interest in this paper.

Although the above results from the two-loop perturbation combined with the ladder approximation are very suggestive, the relevant dynamics is obviously of nonperturbative nature, we would need fully nonperturbative studies. Among others the lattice simulations developed in the lattice QCD would be the most powerful tool to investigate the walking behavior of the large N_f QCD. Actually, there were some pioneering works on the large N_f QCD in somewhat different contexts [10–13], and more recently there have been many lattice studies towards the above problem [14]. The immediate issues are: What is the critical number N_f^{cr}? What is the signature of the walking theory on the lattice? In particular, the above two-loop/ladder studies would suggest that the walking theory if existed might be in between $N_f = 8$ and $N_f = 12$. As to $N_f = 12$ there have been many analyses including those of ourselves which are consistent with the theory being inside the conformal window [10,11,15–24], although some works prefer the SχSB phase [25,26]. There were also simulations on $N_f = 10$ [27] consistent with the infrared conformality. We thus are interested in $N_f = 8$ as a candidate for the walking theory.

Actually, the $N_f = 8$ is particularly interesting from the model-building point of view [28]: A typical technicolor model is the so-called one-family model (Farhi-Susskind model [29]) which has a one-family of colored and uncolored weak-doublet technifermions (techniquarks and technileptons) corresponding to each family of the SM quarks and leptons. It can embed the technicolor gauge and the gauged three generations of the SM fermions into a single gauge group (ETC) and thus is the most straightforward way to accommodate the technifermions and the SM fermions into a simple scheme to give mass to the SM fermions. Thus, if the $N_f = 8$ turns out to be a walking theory, it would be a great message for the phenomenology, which is to be tested by the on-going LHC. Actually, the technidilaton [1,5] in the WTC for the one-family model is consistent with the present LHC data for 125 GeV boson in a ladder analysis [6] and in holographic estimate [6].[2]

If $N_f = 8$ is a walking theory desired for the WTC, it should be inside the SχSB phase $N_f = 8 < N_f^{cr}$ ($m_D \neq 0$)
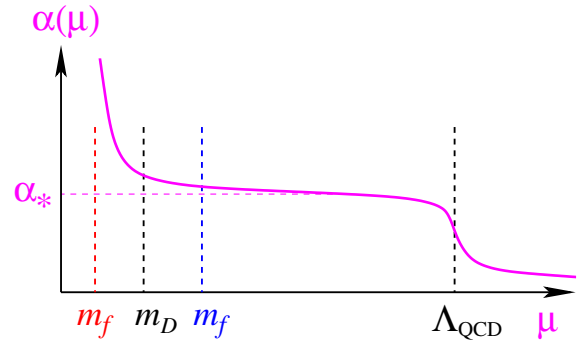

FIG. 1 (color online). Schematic two-loop/ladder picture of the gauge coupling of the massless large N_f QCD as a walking gauge theory in the SχSB phase near the conformal window. m_D is the dynamical mass of the fermion generated by the SχSB. The effects of the bare mass of the fermion m_f would be qualitatively different depending on the cases: Case 1: $m_f \ll m_D$ (red dotted line) well described by ChPT, and case 2: $m_f \gg m_D$ (blue dotted line) well described by the hyper scaling.

and at the same time be close to the phase boundary with the conformal window $N_f > N_f^{cr}$ ($m_D = 0$) such that $m_D \ll \Lambda_{QCD}$. Now the lattice simulations we are making contain several scale-symmetry breaking parameters, the fermion bare mass m_f as well as a finite box L^3 and lattice spacing a, which do not exist in the continuum theory we are interested in. Among others the fermion bare mass m_f obviously distorts the ideal behavior of the breaking of the scale symmetry in a way similar to the continuum theory. Then, disregarding the effects of the lattice parameters L and a for the moment,[3] we may imagine possible effects of the fermion bare mass on the walking coupling of our target of study as in Fig. 1, which is suggested by the two-loop/ladder analysis.

Case 1. $m_f \ll m_D \ll \Lambda_{QCD}$ (red dotted line in Fig. 1): The chiral perturbation theory should hold in a way similar to the real-life QCD with light quarks.

Case 2. $m_D \ll m_f \ll \Lambda_{QCD}$ (blue dotted line in Fig. 1): The conformal hyperscaling relation should hold approximately with a large anomalous dimension $\gamma_m \simeq 1$.

Actually, the SχSB order parameter to be measured on the lattice is not m_D but would be the decay constant F_π of the Nambu-Goldstone boson π extrapolated to the chiral limit: $F = F_\pi(m_f = 0)$ which would be expected roughly the same as m_D: $m_D = \mathcal{O}(F)$.

There is a caveat about the approximate hyperscaling relation to be expected in case 2 ($m_D \ll m_f \ll \Lambda_{QCD}$):

---

[2]As to the immediate questions about the problem with the S, T parameters, see, for example, discussions in Ref. [30].

[3]In our simulation we use the parameter region where the effect of the system size is subdominant compared to the mass effect. This strategy is different from the one which is advocated by the authors of Refs. [23,24].

There are two infrared mass parameters m_D and m_f which violate the infrared conformality and hence the possible hyperscaling relations for the physical mass quantities measured from the spectrum should not be universal but do depend on both of them in nonuniversal ways, in sharp contrast to the hyperscaling relation in the conformal window where all the mass parameters from the spectra reflect the deformation by the unique infrared scale-violating parameter m_f in a universal way. In particular, when m_f is getting close to the region in case 1, where π mass M_π and the other quantities such as ρ mass M_ρ and F_π behave qualitatively different towards the chiral limit: $M_\pi \rightarrow 0$ while the others remain nonzero.

To date, some groups carried out lattice studies on 8-flavors, with Wilson fermions [10,11,23,24] and with staggered fermions [12,15,25,26,31–34]. References [10,11,23,24] concluded the $N_f = 8$ is in the conformal window, but Refs. [12,15,25,26,31,32] concluded that the $N_f = 8$ resides on the chiral broken phase. Even if $N_f = 8$ is in the chiral broken phase, it has not been investigated whether the behavior of this system is QCD-like or the walking with the large anomalous mass dimension.

In this paper we study the meson spectrum by simulating the $N_f = 8$ QCD, based on yet another lattice fermion, the highly improved staggered quark (HISQ) [35], applied to $N_f = 8$ for the first time. Preliminary reports were given in Ref. [36]. HISQ action improves the behavior towards the continuum limit through the improvement of the flavor symmetry. The salient feature of our collaboration is that we have been investigating $N_f = 4, 8, 12, 16$ on the setting of HISQ action with the same systematics in order to study the N_f dependence of the physics systematically [21,36]. Thus, our analyses for $N_f = 8$ are made in comparison with those for other flavors of our group.

We first show the data of the meson spectrum, M_π and F_π, as well as M_ρ and the chiral condensate $\langle \bar{\psi}\psi \rangle$ for $\beta (\equiv 6/g^2) = 3.8$ on the $L^3 \times T$ lattice with $L = 12$–36 and $T = 16$–48, and $m_f = 0.015$–0.16. We find the two regions of m_f having qualitatively different properties: $m_f = 0.015$–0.04 and $m_f = 0.05$–0.16. We analyze the data based on the chiral perturbation theory (ChPT) [37], for small m_f: $m_f = 0.015$–0.04 (roughly corresponding to case 1 in Fig. 1 in the above). We find that the ChPT analysis is self-consistent and find a result consistent with the nonzero value of F and M_ρ and vanishing of M_π in the chiral limit extrapolation based on the ChPT (we also estimate the effects of the chiral logarithm). The chiral condensate is also a nonzero value in the chiral limit extrapolation, which neatly coincides with the Gell-Mann-Oakes-Renner (GMOR) relation obtained from the π data in the chiral limit extrapolation.

As to the large m_f ($m_f = 0.05$–0.16) (roughly corresponding to case 2 in Fig. 1), we find the finite-size hyperscaling (FSHS) [38–41] holds in this region, when we take into account mass corrections to the FSHS. Note that such corrections were sizable [21] in the large mass region even for $N_f = 12$, which are consistent to be in the conformal window. From the hyperscaling analysis for such a large m_f, we find a large anomalous mass dimension $\gamma_m \sim 1$ consistent with that desired by the WTC. This implies that there exists a remnant of the infrared conformality where the spontaneous chiral symmetry breaking (SχSB) effects are negligible compared with the mass deformation m_f. It is the first time that the hyperscaling relation is observed in a theory with SχSB.

The SχSB feature of $N_f = 8$ data near the chiral limit is found to be qualitatively similar to those of the $N_f = 4$ case: We actually find $N_f = 4$ data indicate robust signals of the SχSB phase. On the other hand, our $N_f = 4$ data indicate no trace of the hyperscaling relation for the large m_f region in sharp contrast to $N_f = 8$ data. The $N_f = 8$ result is also contrasted with the $N_f = 12$ where our previous study concluded that the ChPT analysis with our data was not self-consistent, while the FSHS relation held consistently with the infrared conformality.

This suggests that a typical technicolor ("one-family model") as modeled by the $N_f = 8$ QCD can be a walking technicolor theory having an approximate scale invariance with large anomalous dimension.

This article is organized as follows: Sec. II presents our lattice simulation setup, calculation of observables, analysis method, and the results of the crude analysis of our data. Section III shows the analysis based on the ChPT to show that $N_f = 8$ is actually in the SχSB phase. Section IV is to study the remnants of conformality. Section V is devoted to the summary and discussion. Appendices A and B summarize detailed numerical results for $N_f = 8$ and 4, respectively. In Appendix C we estimate chiral log corrections in $N_f = 8$. We analyze FSHS in an alternative method in Appendix D.

II. LATTICE SIMULATION AND THE RESULTS

A. Lattice setup

In our simulation, we use the tree-level Symanzik gauge action and HISQ action [35] without the tadpole improvement and the mass correction in the Naik term [42]. It is expected that the flavor symmetry in the staggered fermion and the behavior towards the continuum limit are improved by HISQ improvement. We carry out the simulation by using the standard hybrid Monte-Carlo (HMC) algorithm using MILC code version 7 [43] with some modifications to suit our needs. One of the modifications is the Hasenbush mass preconditioning [44] to reduce the large computational cost of the configuration generation at the smaller m_f. We measure the mass of the pion M_π, ρ-meson

M_ρ and the decay constant of the pion F_π and the chiral condensate $\langle \bar{\psi}\psi \rangle$ as the basic observable to explore the large-N_f QCD.

The simulation in the preliminary report [36], which includes the study of the anomalous dimension, for $N_f = 8$ is carried out at $\beta(= 6/g^2) = 3.6, 3.7, 3.8, 3.9, 4.0$ for various quark masses and on various lattices, $L^3 \times T$, where L is the spatial size and T the temporal size. We need to choose as small value of β as possible to obtain a large enough physical volume to minimize the finite-volume effect. From the global survey mentioned above, we found that $\beta < 3.8$ is too strong to carry out the HMC simulation with HISQ. Therefore, we choose $\beta = 3.8$ in this article.

Note that the aspect ratio is kept fixed as $T/L = 4/3$, in which $L = 12, 18, 24, 30,$ and 36. The boundary condition in the spatial direction is the periodic and the one in the temporal direction is the antiperiodic for fermions. We take more than 700 trajectories for the ensemble with 4–5 steps for saving the configuration. The error analysis is performed with the standard jackknife analysis having the suitable bin size, 40 trajectories. In the following analyses the error of the fit result is estimated from the standard deviation of least squares coefficients. See the details of the simulation parameter in Tables XII, XIII, XIV, XV, and XVI.

We also generate gauge configurations for $N_f = 4$. From $\beta = 3.6, 3.7, 3.8$ which were investigated in the preliminary study [36], here we focus on $\beta = 3.7$, which is appropriate for our purpose, with high accuracy on $12^3 \times 18$, $16^3 \times 24$, and $20^3 \times 30$. See Appendix B for details.

B. Calculation of observables

We measure the two-point correlation functions of the staggered bilinear pseudoscalar operator which corresponds to the Nambu-Goldstone (NG) mode associated with the chiral symmetry of the staggered fermions. The corresponding spin-flavor structure is $(\gamma_5 \otimes \xi_5)$, denoted by "PS" in Ref. [45]. The random wall source is used for the quark operator for the bilinear, which becomes a noisy estimator of the point bilinear operator with spatial sum at a given time slice t_0. We combine quark propagators solved with periodic and antiperiodic boundary conditions in the temporal direction (see, e.g., Ref. [46]), which is denoted by "P + AP" in this article. In this well-known technique, the temporal size is effectively doubled, which enables us to have sufficient range for the fitting. Denoting such a π correlator as $C_{\text{PS}}(t)$, this behaves as the following expression in the staggered fermion with P + AP prescription:

$$C_{\text{PS}}(t) = C(e^{-M_\pi t} + e^{-M_\pi(2T-t)}) + B(-1)^t, \quad (1)$$

where B is the constant term in the oscillation mode and M_π is the mass of NG-pion mode, and C is the amplitude relating to the decay. Here we use

$$\tilde{C}_{\text{PS}}(2t) = C_{\text{PS}}(2t)/2 + C_{\text{PS}}(2t-1)/4 + C_{\text{PS}}(2t+1)/4. \quad (2)$$

This linear combination kills the constant oscillation mode, which could originate from the single quark line wrapping around the antiperiodic temporal boundary. The mass of NG pion is obtained by the fit of the two-point correlators of $\tilde{C}_{\text{PS}}$ from a random source with double period by a fit function with the fit range $[t_{\min}, T]$,

$$\tilde{C}_{\text{PS}}(2t) = \tilde{C}(e^{-M_\pi 2t} + e^{-M_\pi(2T-2t)}), \quad (3)$$

where $2\tilde{C} = C(1 + \cosh(M_\pi))$.

The pseudoscalar decay constant, F_π, is obtained through the matrix element of the pseudoscalar operator,

$$F_\pi = \frac{m_f}{M_\pi^2} \langle 0|P^a(0)|\pi^a; \vec{p} \rangle, \quad (4)$$

by using the partially conserved axial current (PCAC) relation.[4]

We measure M_ρ from the staggered vector meson operator ($\gamma_i\gamma_4 \otimes \xi_i\xi_4$, denoted by PV in Ref. [45]. The asymptotic form of the PV correlator at large t may be written as

$$C_{\text{PV}}(t) = C_1(e^{-M_\rho t} + e^{-M_\rho(2T-t)}) + C_2(-1)^t(e^{-M_{a_1}t} + e^{-M_{a_1}(2T-t)}), \quad (5)$$

where M_{a_1} corresponds to the mass of the axial vector meson which is the parity partner mode of PV mode in the staggered fermion. Since there exists a constant mode due to the wrapping-around effect, we use

$$\tilde{C}_{\text{PV}}(2t) = C_{\text{PV}}(2t)/2 + C_{\text{PV}}(2t-1)/4 + C_{\text{PV}}(2t+1)/4. \quad (6)$$

Therefore,

$$\tilde{C}_{\text{PV}}(2t) = \tilde{C}_1(e^{-M_\rho 2t} + e^{-M_\rho(2T-2t)}) + \tilde{C}_2(e^{-M_{a_1}2t} + e^{-M_{a_1}(2T-2t)}), \quad (7)$$

where $2\tilde{C}_1 = C_1(1 + \cosh(M_\rho))$ and $2\tilde{C}_2 = C_2(1 - \cosh(M_{a_1}))$. Even in the case of $M_\rho \simeq M_{a_1}$ and $C_1 \simeq C_2$, we have $\tilde{C}_1 \gg \tilde{C}_2$ for our typical value of M_ρ. Then Eq. (7) can be approximated to the simple cosh function of the two-point correlators of $\tilde{C}_{\text{PV}}$:

$$\tilde{C}_{\text{PV}}(2t) = \tilde{C}_1(e^{-M_\rho 2t} + e^{-M_\rho(2T-2t)}), \quad (8)$$

and we obtain M_ρ.

Besides these main channels, we study the masses of mesons interpolated from local operators, a non-NG channel ($\gamma_5\gamma_4 \otimes \xi_5\xi_4$) denoted by "SC," and a vector meson ($\gamma_i \otimes \xi_i$) denoted by "VT" in Ref. [45], by which we will

---

[4]We use the convention as $F_\pi = \sqrt{2}f_\pi$, where $f_\pi = 93$ [MeV] in the real-life QCD.
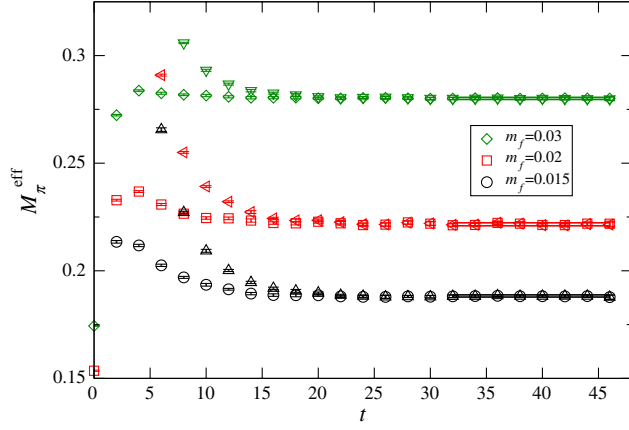
FIG. 2 (color online). Effective masses of PS meson, M_π^{eff}, at $L = 36$. Triangles and other symbols denote results from point sink correlators with random wall source and corner wall source, respectively. Fit results with error band obtained from random wall source correlator are also plotted by solid lines.

show that the flavor-symmetry breaking is small in HISQ. These masses are obtained from the corner wall source correlator.

The effective masses are calculated through $\tilde{C}_{\text{PS}}(2t)$ defined in Eq. (2). Figure 2 shows typical examples of PS channel for the largest volume. The horizontal lines show the results of fitting $\tilde{C}_{\text{PS}}(2t)$ with Eq. (3) with $32 \leq 2t \leq 48$, where a plateau is observed. All the fit results are summarized in Tables XII, XIII, XIV, XV, and XVI.

We also calculate the chiral condensate $\langle \bar{\psi} \psi \rangle$ normalized for a single Dirac flavor which can be obtained through

$$\langle \bar{\psi}(x) \psi(x) \rangle = \frac{1}{4} \text{Tr}[D_{\text{HISQ}}^{-1}(x, x)], \qquad (9)$$

where $D_{\text{HISQ}}(x, y)$ is the single species (four flavor) staggered Dirac operator for HISQ. Here an average over the space-time x is calculated through a stochastic method.

C. Analysis methods

We performed the analysis based on the chiral perturbation theory (ChPT) and the (finite-size) hyperscaling, as explained in the following: If the system is in the spontaneous chiral symmetry broken (SχSB) phase, physical quantities in the spectroscopy, M_H for $H = \pi, \rho, \ldots$ and F_π, are described by the ChPT. The mass and decay constant of π depend on m_f up to chiral log as

$$\begin{aligned} M_\pi^2 &= C_1^\pi m_f + C_2^\pi m_f^2 + \cdots, \\ F_\pi &= F + C_1^F m_f + C_2^F m_f^2 + \cdots, \end{aligned} \qquad (10)$$

where F is the value in the chiral limit.

On the other hand, if the theory is in the conformal window, M_H and F_π obey the conformal hyperscaling [47]

$$M_H \propto m_f^{\frac{1}{1+\gamma_*}}, \qquad F_\pi \propto m_f^{\frac{1}{1+\gamma_*}}, \qquad (11)$$

where γ_* denotes the mass anomalous dimension γ_m at the infrared fixed point and its value is universal for all channels. On the finite volume M_H and F_π are described by the finite size hyperscaling (FSHS) [38–41] on dimension-less quantities

$$\xi_p \equiv L M_p \quad \text{for } p = \pi \quad \text{or} \quad \rho, \qquad (12)$$

or

$$\xi_F \equiv L F_\pi, \qquad (13)$$

given as

$$\xi_H = \mathcal{F}_H\left(L m_f^{\frac{1}{1+\gamma_*}}\right), \qquad (14)$$

where $H = \pi, \rho$ or F. The function, $\mathcal{F}_H$, is a function (unknown *a priori*) of the scaling variable $X = L m_f^{\frac{1}{1+\gamma_*}}$.

D. Results

Spectral quantities, such as M_π, M_ρ, F_π, $\langle \bar{\psi} \psi \rangle$, are calculated on the gauge field ensembles for the $N_f = 8$ QCD at $\beta = 3.8$, as described in Sec. II. The m_f dependence of the results is shown in Fig. 3. Large finite size effect is observed for the smaller m_f region on $L = 12$.

The expected good flavor symmetry in HISQ action is actually observed in near degeneracy of PS and SC, and of PV and VT. See Fig. 4.

Before giving the in-depth analyses in the following sections, let us perform some crude analysis here. Spontaneous chiral symmetry breaking leads to nonzero F_π and M_ρ while vanishing M_π in the chiral limit. Thus, the ratios F_π / M_π and M_ρ / M_π should diverge in the chiral limit. On the other hand, in the conformal phase the ratios should take a constant value near the chiral limit as implied by the hyperscaling relation in Eq. (11).

Now look at Figs. 5 and 6 which show that the ratio increases monotonically towards the chiral limit, if one takes the largest volume data at each M_π. This resembles the $N_f = 4$ case where SχSB is clearly observed and shows clear contrast against the same plot for $N_f = 12$ which are consistent with conformality. This strongly suggests that $N_f = 8$ QCD is in SχSB phase. In order to further study the chiral property of $N_f = 8$, we carry out ChPT analysis in the next section.

III. CHIRAL PERTURBATION THEORY ANALYSIS

In order to carry out the ChPT analysis, the finite volume effect has to be taken into account. Figure 7 shows the spatial size L dependence of F_π, M_π, and M_ρ plotted from the data in Tables XII, XIII, XIV, XV, and XVI. We find that the data on the largest two volumes, at least in this m_f
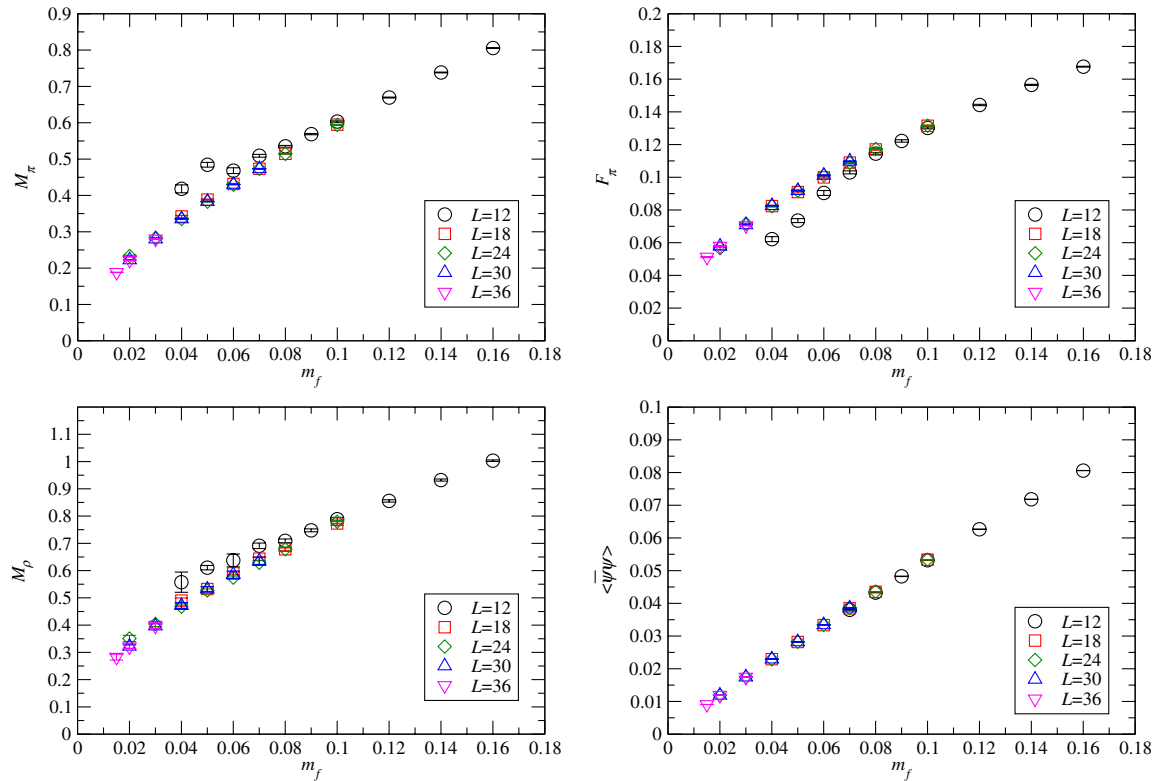
FIG. 3 (color online).   Raw data of observables as a function of m_f for M_π (top left), F_π (top right), M_ρ (bottom left), and $\langle \bar{\psi} \psi \rangle$ (bottom right).

range, are consistent with each other. For the lightest m_f, since there is only one volume data, we cannot study the finite size effect. We, however, find that the LM_π in the lightest m_f is bigger than the one of $m_f = 0.02$ at $L = 30$ (see, Table XV) where the finite size effect is negligible. In the following analysis we understand that there is no finite

FIG. 4 (color online).   Comparisons of M_π and M_{SC}, and of $M_{\rho(PV)}$ and $M_{\rho(VT)}$ as a function of m_f with largest volume data at each m_f.

size effect in the lightest m_f. Therefore, we use the data on the largest lattice at each m_f and perform the infinite volume ChPT analysis.

A. Quadratic fit of F_π

Let us analyze the behavior of F_π, towards the chiral limit. Figure 8 shows the result of F_π at each m_f. We perform the quadratic fit for F_π by varying the fit range of m_f. (We will estimate the effect of the chiral log corrections later.) The quadratic fit result of F_π is written in Table I. As seen in Fig. 8 and Table I, F is nonzero (~ 0.03). Particularly for the small region, $0.015 \leq m_f \leq 0.04$, the polynomial fit gives the good $\chi^2/\mathrm{dof}(= 0.46)$. When we include the data at $m_f = 0.05$, χ^2/dof jumps up. Although this jump might be caused by the instability due to small dof $= 2$, the large χ^2/dof persists for the range with larger masses, thus, with the value of χ^2/dof being more reliable. This suggests that there is a bound, beyond which the ChPT does not describe the data well, and that bound is around $m_f \lesssim 0.05$. With this consideration and the good chiral behavior observed for other quantities for $m_f = 0.015$–0.04, which we will see below, we chose $m_f = 0.015$–0.04 for the fitting range of all quantities.

For the consistency of the ChPT particularly for the large N_f QCD, the expansion parameter [48] for the given M_π is defined as
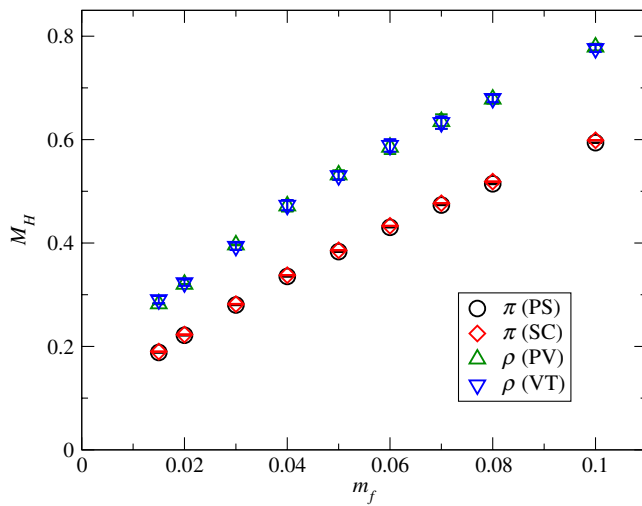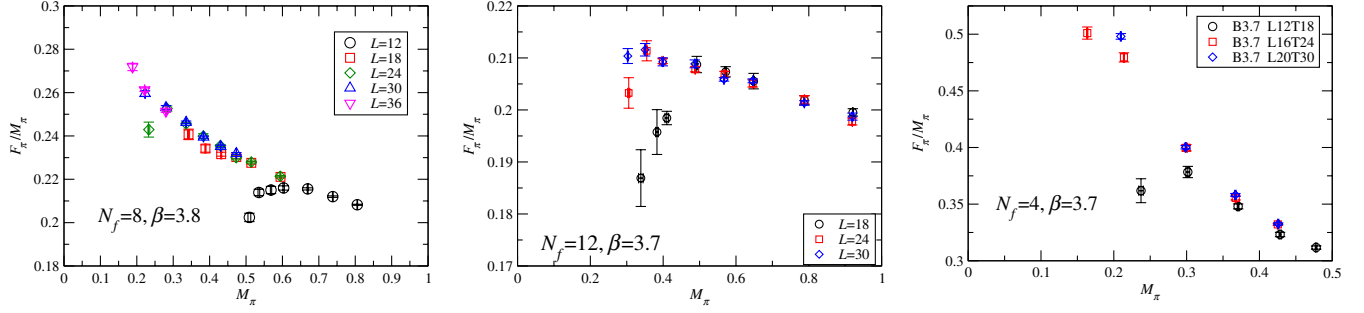
FIG. 5 (color online). F_π/M_π as a function of M_π for $N_f = 8$ (left), $N_f = 12$ at $\beta = 3.7$ (center) in Ref. [21], and $N_f = 4$ at $\beta = 3.7$ (right).
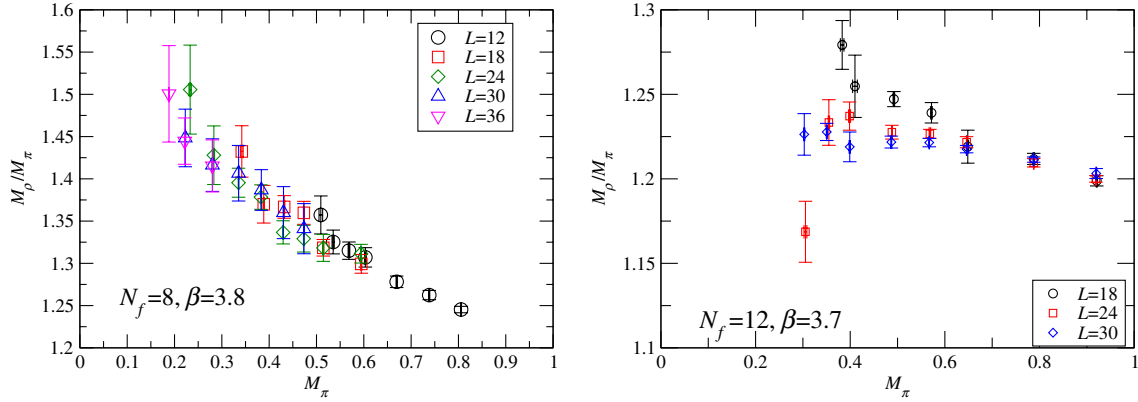

FIG. 6 (color online). M_ρ/M_π as a function of M_π for $N_f = 8$ (left) and $N_f = 12$ at $\beta = 3.7$ (right) in Ref. [21].
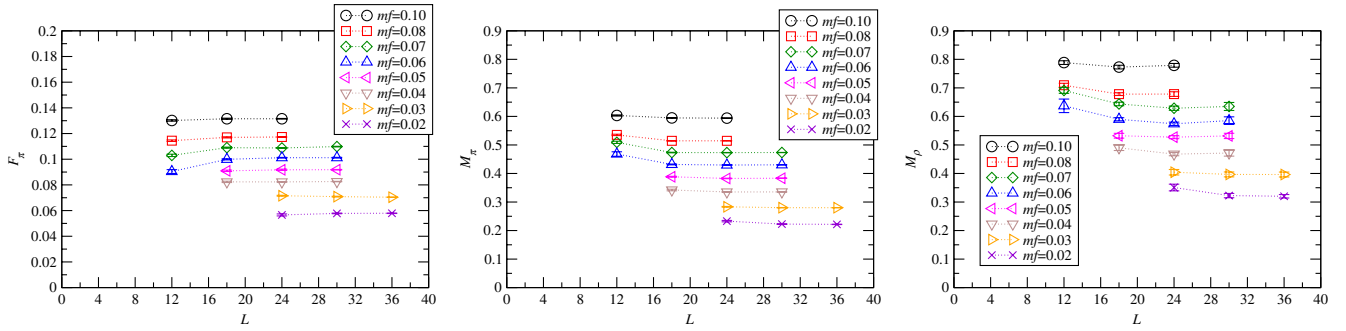

FIG. 7 (color online). F_π (left), M_π (center), and M_ρ (right) as functions of L.

$$\mathcal{X} = N_f\left(\frac{M_\pi}{4\pi F/\sqrt{2}}\right)^2, \qquad (15)$$

and this quantity is required to satisfy the condition $\mathcal{X} < 1$, which, however, could become easily violated when the simulation is made for heavy M_π compared to F. We have $\mathcal{X} = O(1)$ in our smallest m_f. Thus, the ChPT is barely self-consistent in contrast to the case of $N_f = 12$ where $\mathcal{X} \simeq 40$ [21].

The above analysis suggests that our result in $N_f = 8$ is consistent with SχSB phase with

$$F = 0.0310(13) \qquad (16)$$

up to chiral log. Effects of the chiral log will be discussed later.

B. Quadratic fits of M_ρ and M_π^2

Here, we attempt the quadratic fit of M_ρ and M_π^2 to see whether $M_\rho \neq 0$ and $M_\pi^2 = 0$ in the chiral limit.

Figure 9 and Table II are the quadratic fit result of M_ρ. The chiral limit value of M_ρ ($= C_0^\rho$) is estimated using the fitting range $0.015 \leq m_f \leq 0.04$,

FIG. 8 (color online). Results of quadratic fit of F_π for various fit ranges.
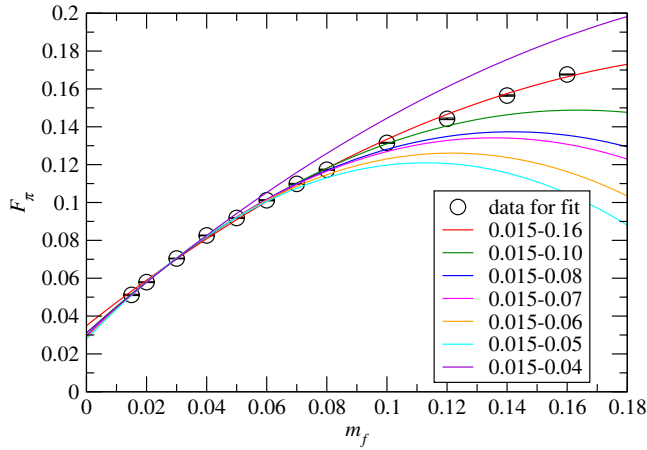

FIG. 9 (color online). Results of quadratic fit of M_ρ for various fit ranges.

$$M_\rho = 0.168(32). \qquad (17)$$

The left panel of Fig. 10 shows M_π^2 and the right panel M_π^2/m_f as a function of m_f. The M_π^2/m_f goes to constant towards the chiral limit, which is consistent with the leading ChPT behavior. However, the visible slope is observed, indicating that there are higher order corrections. This is in contrast to $N_f = 4$ shown in Fig. 20. We analyze M_π^2 by the quadratic fit with the constant term to see whether this constant term becomes zero or not. The result is shown in Fig. 11. In the fitting region $0.015 \leq m_f \leq 0.04$ the constant term is consistent with zero as presented in Table III. Therefore the chiral property of M_ρ and M_π is also consistent with that of SχSB.

C. Chiral condensate

In this subsection, we analyze the chiral condensate, which is an order parameter of SχSB. We perform a direct measurement of the chiral condensate $\langle \bar\psi \psi \rangle = \mathrm{Tr}[D_{\mathrm{HISQ}}^{-1}(x, x)]/4$ and compare it with the quantity

$$\Sigma \equiv \frac{F_\pi^2 M_\pi^2}{4m_f}, \qquad (18)$$

which, in the chiral limit, should coincide with the chiral condensate through the Gell-Mann-Oakes-Renner
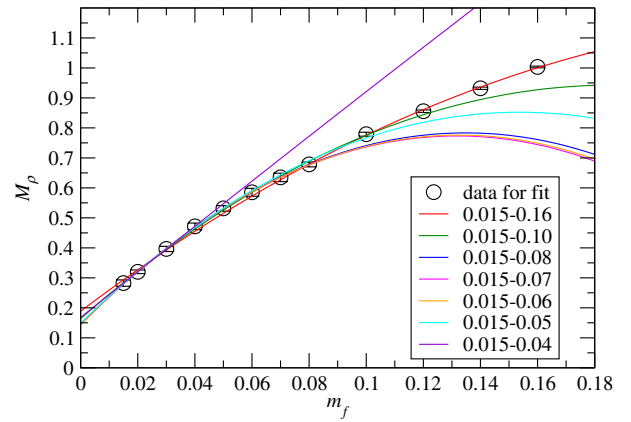
(GMOR) relation. Figure 12 shows the $\langle \bar\psi \psi \rangle$ and Σ for each m_f. We carry out the quadratic fits for each quantity, whose results are summarized in Table IV and shown in Fig. 13. The chiral extrapolations for $\langle \bar\psi \psi \rangle$ and Σ give good values of χ^2/dof only in the small m_f region $0.015 \leq m_f \leq 0.04$, though the dof is too small. Both results in the chiral limit are nonzero, and are consistent with each other, see Fig. 14:

$$\langle \bar\psi \psi \rangle|_{m_f \to 0} = 0.00052(5), \qquad \Sigma|_{m_f \to 0} = 0.00059(13). \qquad (19)$$

We also estimate the chiral condensate in the chiral limit by multiplying F in Eq. (16) with the value of M_π^2/m_f in the chiral limit obtained from the linear fit in Table IV:

$$F^2 \cdot \left(\frac{M_\pi^2}{4m_f}\right)\Big|_{m_f \to 0} = 0.00050(3), \qquad (20)$$

which is consistent with those from the direct and indirect measurements.

From the analyses up to chiral log of all the observables, F_π, M_π, M_ρ and the chiral condensate, we find that the chiral property of $N_f = 8$ QCD is consistent with that of SχSB.

TABLE I. Results of chiral fit of F_π with $F_\pi = F + C_1 m_f + C_2 m_f^2$ for various fit ranges.

Fit range (m_f)	F	$X(m_f^{\mathrm{min}} = 0.015)$	$X(m_f = m_{\mathrm{max}})$	χ^2/dof	dof
0.015–0.04	0.0310(13)	3.74	11.80	0.46	1
0.015–0.05	0.0278(8)	4.64	19.28	5.56	2
0.015–0.06	0.0284(6)	4.44	23.2	4.09	3
0.015–0.07	0.0293(5)	4.18	26.5	4.46	4
0.015–0.08	0.0296(4)	4.10	30.6	4.06	5
0.015–0.10	0.0311(3)	3.70	37.0	7.85	6
0.015–0.16	0.0349(2)	2.94	54.0	34.2	9

TABLE II. Chiral fit of M_ρ with $M_\rho = C_0^\rho + C_1^\rho m_f + C_2^\rho m_f^2$ for various fit ranges.

Fit range (m_f)	C_0^ρ	χ^2/dof	dof
0.015–0.04	0.168(32)	0.0017	1
0.015–0.05	0.149(33)	0.098	2
0.015–0.06	0.145(25)	0.084	3
0.015–0.07	0.144(20)	0.063	4
0.015–0.08	0.146(16)	0.052	5
0.015–0.10	0.164(12)	0.57	6
0.015–0.16	0.189(7)	1.48	9

FIG. 11 (color online). Quadratic fit of M_π^2 for various fit ranges.
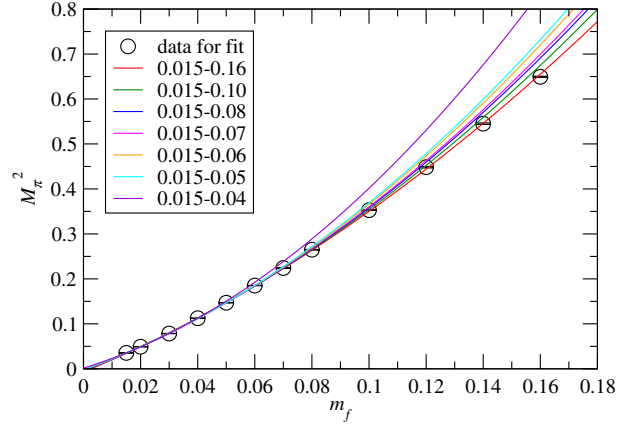
D. Chiral log corrections

So far we have not included the logarithmic correction in the chiral fits. Here we estimate such effects as systematic errors on our previous results.

The logarithmic m_f dependence is predicted by the next leading order (NLO) ChPT for both the M_π^2/m_f and F_π [37], whose formulas are given by

$$\frac{M_\pi^2}{m_f} = 2B\left(1 + \frac{x}{N_f}\log(x) + c_3 x\right) \qquad (21)$$

$$F_\pi = F\left(1 - \frac{N_f x}{2}\log(x) + c_4 x\right), \qquad (22)$$

where the expansion parameter is denoted by $x = 4Bm_f/(4\pi F)^2$, and B, F, c_3, and c_4 are the low energy constants. Our data do not have such logarithmic dependence even in the lightest m_f region as shown in the previous subsections. Actually, such a fit leads to a large χ^2. This is due to the fact that our m_f is much heavier than the region where the NLO ChPT is applicable. The log correction of the F_π, however, is enhanced by the N_f [Eq. (22)], so that the F might be largely affected by this correction, especially in this large N_f theory. Thus, we attempt to estimate the size of the correction by matching our polynomial fit results to the NLO ChPT at m_f such that

$\mathcal{X} = 1$, with $\mathcal{X}$ defined in Eq. (15) where F should read the reestimated one in this analysis. The details of the analysis are explained in Appendix C. A reasonable value of the $\mathcal{X} \lesssim 1$ is realized only in the region, $m_f \lesssim 0.002$, much lighter than the m_f used in our simulation. From the analysis we find that the log correction reduces the value of F by about 30% from the result with quadratic fit.

The other low energy constants including B are obtained simultaneously. The log correction of the chiral condensate is estimated from the GMOR relation, $\langle\bar{\psi}\psi\rangle|_{m_f\to 0} = BF^2/2$, where the values of F and B estimated in this analysis are used. We find that the chiral condensate is reduced by roughly half from the result with quadratic fit by the log correction.

Apart from the log correction, we also estimate the systematic error from other sources. While we adopted the quadratic chiral fits for F and $\langle\bar{\psi}\psi\rangle|_{m_f\to 0}$, linear fits work with reasonable χ^2 with the same fitting range. The differences are counted as systematic errors. For the chiral condensate, the largest difference from the result with the direct measurement to one of the indirect measurements is counted as a systematic error.
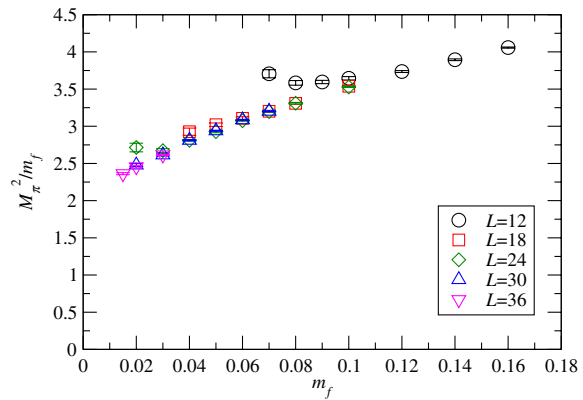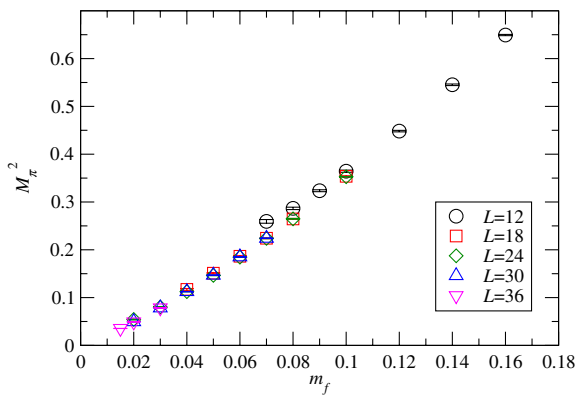

FIG. 10 (color online). M_π^2 (left) and M_π^2/m_f (right) as functions of m_f.

TABLE III. Chiral fit results for M_π^2 with $M_\pi^2 = C_0^\pi + C_1^\pi m_f + C_2^\pi m_f^2$ for various fit ranges.

Fit range (m_f)	C_0^π	χ^2/dof	dof
0.015–0.04	0.0016(13)	1.21	1
0.015–0.05	−0.0017(9)	5.90	2
0.015–0.06	−0.0022(6)	4.18	3
0.015–0.07	−0.0032(5)	5.00	4
0.015–0.08	−0.0037(5)	5.44	5
0.015–0.10	−0.0049(4)	7.28	6
0.015–0.16	−0.0071(3)	14.8	9

The results for the decay constant and the chiral condensate at the chiral limit in this work are

$$F = 0.031(1)\binom{+2}{-10}, \qquad (23)$$

$$\langle \bar\psi \psi \rangle|_{m_f \to 0} = 0.00052(5)\binom{+8}{-29}, \qquad (24)$$

where the first and second errors are statistical and systematic ones, respectively. The lower systematic errors are coming from the log corrections, while the upper ones from the others.

It would be useful to estimate physical quantities in units of the F, because in the technicolor model the F is related to the weak scale,

$$\sqrt{N_d}F/\sqrt{2} = 246 \text{ GeV}, \qquad (25)$$

where N_d is the number of the fermion weak doublets as $1 \leq N_d \leq N_f/2$. From our result, the ratio M_ρ/F in the chiral limit is given as

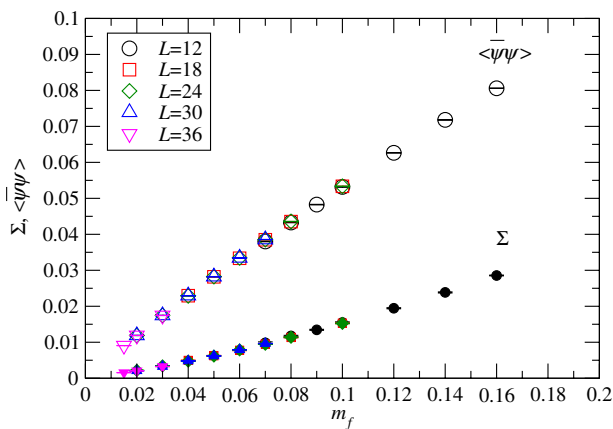$$\frac{M_\rho}{F/\sqrt{2}} = 7.7(1.5)\binom{+3.8}{-0.4}, \qquad (26)$$

FIG. 12 (color online). $\langle \bar\psi \psi \rangle$ [Eq. (9)] and Σ [Eq. (18)] as a function of m_f. The open symbol represents $\langle \bar\psi \psi \rangle$ and the filled symbol is Σ.

where the M_ρ in the chiral limit is the result of the quadratic fit in Eq. (17).

In this analysis we observe the large corrections of the chiral log term in ChPT. In order to reduce the systematic error of the chiral extrapolation and to obtain more accurate predictions in this theory, we will need simulations at the smaller m_f region on larger volumes.

IV. STUDY OF REMNANTS OF CONFORMALITY

In the previous section we showed that the $N_f = 8$ theory is in the SχSB phase. However, if this theory is near the conformal phase boundary, it is expected that some remnants of the conformal symmetry appear in physical quantities.

Here we start with an analysis of F_π from a different point of view. In the conformal phase the F_π obeys the hyperscaling relation in the infinite volume, Eq. (11). We perform the power fit $F_\pi = C_1 m_f^{1/(1+\gamma)}$ with various m_f ranges, where C_1 and γ are free parameters. The numerical results of the power fit are summarized in Table V.

The power fit does not work in the lightest m_f region, $0.015 \leq m_f \leq 0.04$, in which the F_π is consistent with ChPT analysis and the F is nonzero as presented in the previous section. On the other hand, it is remarkable that the fit results in the mass range, $m_f \gtrsim 0.05$, are consistent with the power behavior, the same way as the hyperscaling relation. Furthermore the estimated γ is stable in the larger mass region (see the bottom part of Table V), the property expected from hyperscaling. This suggests that, although $N_f = 8$ QCD is in the SχSB phase, there exists a remnant of the conformality. Therefore, in this section, we will carry out further in depth analysis, which employs the hyperscaling test on the finite volume for F_π as well as M_π and M_ρ, to investigate whether the remnant of the conformality really persists.

A. Finite size hyperscaling test

If the system is in the conformal window, the data on a finite volume is in good agreement with the finite size hyperscaling (FSHS) having a universal value of $\gamma = \gamma_*$ at IRFP for observables as given in Eq. (14). In general our data of $N_f = 8$ cannot satisfy the FSHS with universal γ in the whole range of m_f, because we showed that the theory is in the SχSB phase as analyzed in Sec. III. However, because of the power behavior in the middle range of the fermion mass as mentioned in the above, we carry out the FSHS test in our data to find a remnant of the conformality.

For this test, we plot the observables, ξ_F [Eq. (13)], ξ_π, and ξ_ρ [Eq. (12)], as functions of $X = Lm_f^{1/(1+\gamma)}$ with changing the value of γ. Figures 15–17 are the results of the FSHS test of ξ_F, ξ_π, and ξ_ρ for various γ's: The data are aligned (collapsing) at around $\gamma = 1.0$, 0.6, and 0.8, respectively. The optimal values of γ for the observables

TABLE IV. Chiral condensate in the chiral limit: The quadratic fit result of $\langle \bar{\psi}\psi \rangle$ and Σ in various fit ranges. $\langle \bar{\psi}\psi \rangle = C_0^{\langle \bar{\psi}\psi \rangle} + C^{\langle \bar{\psi}\psi \rangle}m_f + C_2^{\langle \bar{\psi}\psi \rangle}m_f^2$. $\Sigma = C_0^{\Sigma} + C_1^{\Sigma}m_f + C_2^{\Sigma}m_f^2$. The linear fit of $M_\pi^2/m_f = C_0^{(M_\pi^2/m_f)} + C_1 m_f$ yields the combination $F^2 M_\pi^2/(4m_f) \rightarrow F^2 C_0^{(M_\pi^2/m_f)}/4$ in the chiral limit.

Fit range	$C_0^{\langle \bar{\psi}\psi \rangle}$			C_0^{Σ}			$C_0^{(M_\pi^2/m_f)}$			
(m_f)	Value	χ^2/dof	dof	Value	χ^2/dof	dof	Value	χ^2/dof	dof	$F^2 C_0^{(M_\pi^2/m_f)}/4$
0.015–0.04	0.00052(5)	2.65	1	0.00059(13)	1.11	1	2.087(18)	1.34	2	0.00050(3)
0.015–0.05	0.00037(3)	11.5	2	0.00015(9)	11.5	2	2.126(14)	5.22	3	0.00041(17)
0.015–0.06	0.00037(2)	7.70	3	0.00007(7)	8.12	3	2.151(11)	6.07	4	0.00043(13)
0.015–0.07	0.00039(2)	6.51	4	0.00002(6)	6.56	4	2.186(10)	11.4	5	0.00047(11)
0.015–0.08	0.00041(2)	6.23	5	−0.00003(6)	6.22	5	2.204(9)	14.2	6	0.00048(9)
0.015–0.10	0.00041(2)	5.19	6	−0.00013(4)	6.75	6				
0.015–0.16	0.00056(1)	18.9	9	−0.00026(3)	7.19	9				

are not universal in this estimate, in contrast to $N_f = 12$, where the alignments was observed with almost universal γ [21]. It is also noted the existence of alignment for each observable is in contrast to $N_f = 4$, where no alignment is observed (see Appendix B).

Since Figs. 15–17 show the good linear behavior, we carry out a linear fit as the leading approximation of FSHS,

$$\xi_H = C_0^H + C_1^H X, \qquad (27)$$

for each observable. This formula becomes the hyperscaling, Eq. (11) in the infinite volume limit. In Sec. III we saw the ChPT fit worked well for the smallest mass region $m_f \lesssim 0.04$ for all the observables. On the other hand, we already showed the powerlike behavior of the F_π for larger masses $m_f \gtrsim 0.05$. Thus, we restrict ourselves to fit the data in $m_f \gtrsim 0.05$ in this analysis. To have good linearity we restrict the data in the larger ξ_π region, $\xi_\pi \gtrsim 8$.

Panels in Fig. 18 are the fit result of FSHS for ξ_π, ξ_F, and ξ_ρ from the left to the right. The fitting result is given in Table VI, which is consistent with the $P(\gamma)$ analysis that does not assume the functional form of fitting given in Appendix D. In Fig. 18 data included in the fit are shown as filled symbols, while those with open symbols are not

included. The figures show the linear fit works well for ξ_ρ (χ^2/dof $= 0.66$) and ξ_F (χ^2/dof $= 0.73$), while the fit for ξ_π has χ^2/dof $= 2.52$.

The larger χ^2/dof of the ξ_π fit might be caused by corrections which are not explained by the simple fit form in Eq. (27). To check the existence of the correction, we fit the data of ξ_π only on two volumes, and slide the range of the volumes to investigate the fit range dependence of the γ. The resulting χ^2/dof, tabulated in Table VII, is better than the above fit. The results seem to have a tendency to decease the γ as the volume decreased. The maximum and minimum results deviate from each other by more than 2 standard deviations, and they also differ from the result using the four volumes tabulated in Table VI. This tendency would suggest that there are corrections to the leading behavior of the FSHS in Eq. (27), but it is not clear that this tendency comes from only a finite volume effect, because the range of the m_f is also changed as the volume. On the other hand, the results for the ξ_F and ξ_ρ in Table VII are consistent with each result tabulated in Table VI, so that we do not expect that there are significant corrections in these data.

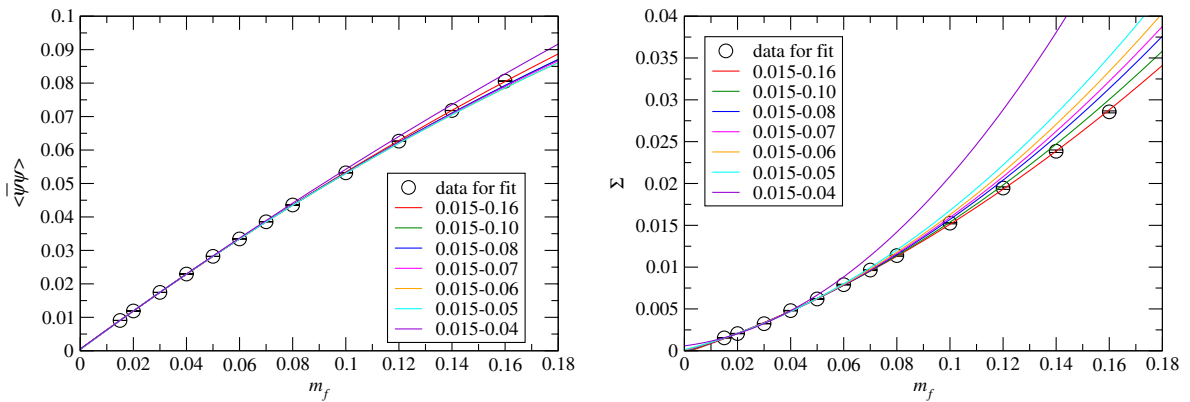We will discuss the types of the corrections of Eq. (27) in the next subsection.

FIG. 13 (color online). Quadratic fits of $\langle \bar{\psi}\psi \rangle$ (left) and Σ (right).
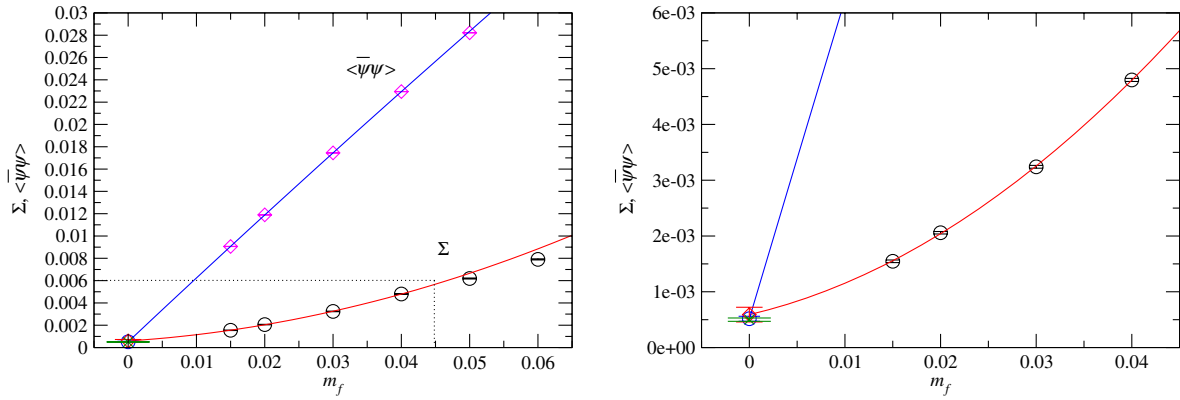
FIG. 14 (color online). Σ and $\langle \bar{\psi} \psi \rangle$ (left panel) as a function of m_f. The small region, $0 \leq m_f \leq 0.045$ and $0 \leq \Sigma, \langle \bar{\psi} \psi \rangle \leq 0.0006$, in the left panel is enlarged to the right panel. The quadratic fit curves by using the data in $0.015 \leq m_f \leq 0.04$ are shown. The green symbol is the value in Eq. (20).

B. FSHS fits with the correction term

Since $N_f = 8$ theory is in SχSB phase, FSHS cannot become accurate by approaching to the chiral limit, which is in contrast to the $N_f = 12$ where FSHS does [21]. Therefore FSHS is only expected for the larger mass region, where mass corrections may not be negligible. In fact, in the last subsection the decreasing tendency of the $\gamma(M_\pi)$ depending on the fit range is seen, which might suggest that there are corrections in the simple FSHS form in Eq. (27), To include mass corrections we assume the same fitting forms as in the $N_f = 12$ case [21] as

$$\xi_H = C_0^H + C_1^H X + C_2^H L m_f^\alpha. \tag{28}$$

TABLE V.   Power fit results of F_π for various fit ranges, using $F_\pi = C_1 m_f^{1/(1+\gamma)}$. The top part of the table shows the results for the ranges with minimum mass set to the lightest, $m_f = 0.015$, while the bottom does those with maximum mass being the heaviest $m_f = 0.16$.

Fit range (m_f)	C_1	γ	χ^2/dof
0.015–0.04	0.415(7)	0.988(19)	14.8
0.015–0.05	0.414(5)	0.991(15)	9.84
0.015–0.06	0.418(4)	0.979(12)	7.88
0.015–0.07	0.424(3)	0.963(9)	7.35
0.015–0.08	0.425(3)	0.961(8)	6.15
0.015–0.10	0.426(2)	0.958(7)	5.31
0.015–0.16	0.428(1)	0.952(4)	3.98
0.02–0.16	0.429(1)	0.947(4)	2.22
0.03–0.16	0.431(1)	0.942(5)	1.94
0.04–0.16	0.429(2)	0.950(10)	1.23
0.05–0.16	0.431(2)	0.941(7)	0.66
0.06–0.16	0.429(2)	0.948(9)	0.44
0.07–0.16	0.429(3)	0.950(10)	0.52
0.08–0.16	0.431(3)	0.939(14)	0.20
0.10–0.16	0.432(4)	0.934(19)	0.23

Since it is hard to determine the exponent α of the correction term when the fit is performed for each observable individually, we fix it in our analysis. Among various choices of the α, we take two values: $\alpha = 1$ and 2. The first choice $\alpha = 1$ is regarded as an m_f correction in the heavy region, and the second one $\alpha = 2$ may be identified as a $\mathcal{O}(a^2)$ discretization effect.

Using the fit assumptions we fit each observable with the same data region as in the last subsection, $m_f \gtrsim 0.05$ and $\xi_\pi \gtrsim 8$. The results are tabulated in Table VIII. The fit results with both $\alpha = 1$ and 2 of the ξ_π show the correction term actually takes effect ($C_2^\pi \neq 0$), with reasonable χ^2/dof. Because of the large correction, the γ of the ξ_π is largely changed from the one without the correction term in Table VI, especially in the $\alpha = 1$ case, and the value becomes closer to the ones from the other observables. On the other hand, for the ξ_F and ξ_ρ fits, it is found that the correction is negligible, and the resulting γ's are consistent with the ones without the correction, presented in Table VI, as expected in the analyses in the last subsection. While in the $\alpha = 1$ case, we obtain reasonable consistency of the γ from the three observables within less than 2 standard deviations, we cannot exclude the $\alpha = 2$ fit. Thus, the above analyses would suggest $\gamma = 0.62$–0.97 depending on the observables and also the form of the correction term.

Since we observed that the values of γ with Eq. (28) for all the observables become closer to each other than those without the correction terms, it might be possible to obtain a common value of the γ from all the observables using the fit including the correction. Thus, we perform a simultaneous fit using all the observables M_π, F_π, and M_ρ with a common γ. For simplicity, we assume the absence of the statistical correlations between each data of M_π, F_π, and M_ρ. In the fit we do not fix the value of the α, and treat it as a free parameter. It is expected that the corrections are small in the ξ_F and ξ_ρ, so that we first carry out a fit

FIG. 15 (color online). ξ_F plotted as functions of X with $\gamma = 0.6$ (left), 1.0 (center), and 1.4 (right) for the FSHS test.

FIG. 16 (color online). ξ_π plotted as functions of X with $\gamma = 0.2$ (left), 0.6 (center), and 1.0 (right) for the FSHS test.
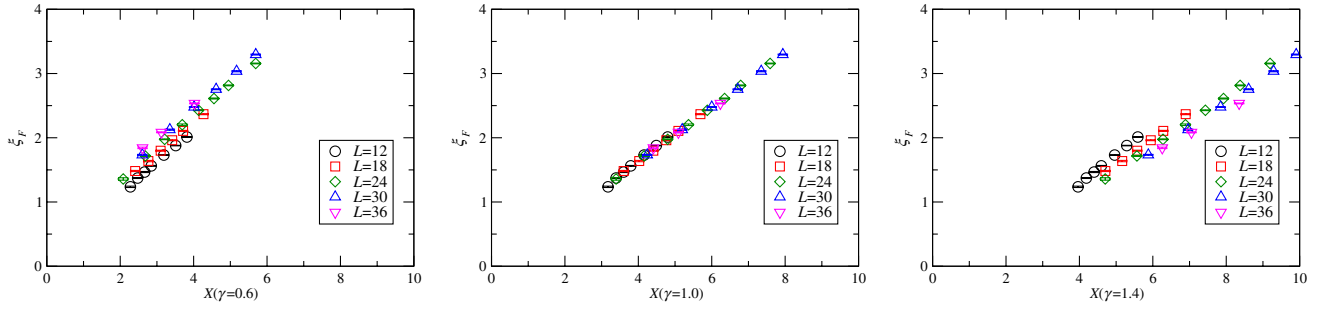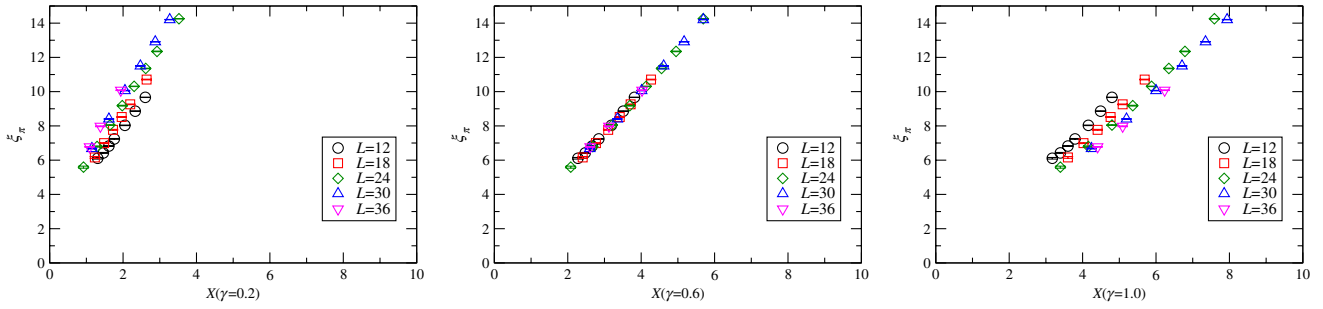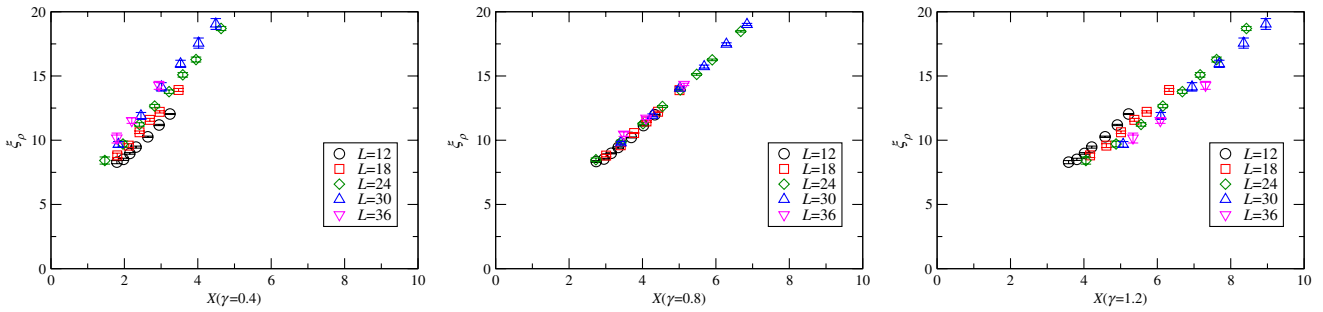

FIG. 17 (color online). ξ_ρ plotted as functions of X with $\gamma = 0.4$ (left), 0.8 (center), and 1.2 (right) for the FSHS test.
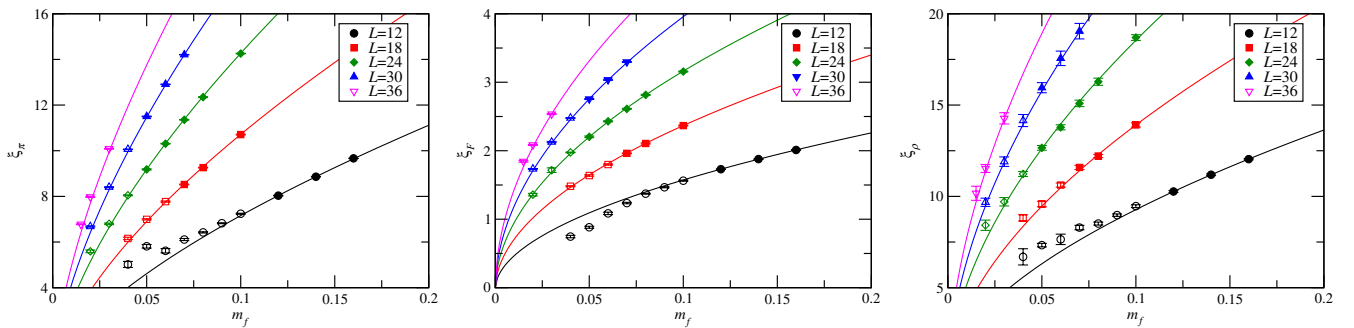

FIG. 18 (color online). Linear fits for the FSHS of M_π (left), F_π (center), and M_ρ (right). The filled symbols are included in the fit, but the open symbols are omitted. The fitted region is $m_f \geq 0.05$ and $\xi_\pi \geq 8$.

TABLE VI. The γ fitted by the linear ansatz. The fitted region is $m_f \geq 0.05$ and $\xi_\pi \geq 8$.

	γ	C_0^H	C_1^H	χ^2/dof
ξ_π	0.5668(26)	0.049(22)	2.57766(99)	2.52
ξ_F	0.9279(79)	$-0.17(10)$	0.4372(38)	0.73
ξ_ρ	0.798(20)	0.04(19)	2.779(69)	0.66

TABLE VII. The γ fitted by the linear ansatz using the data on two volumes.

		ξ_π		ξ_F		ξ_ρ
L	γ	χ^2/dof	γ	χ^2/dof	γ	χ^2/dof
(30,24)	0.5864(61)	1.09	0.948(18)	1.19	0.84(11)	0.62
(24,18)	0.5720(88)	0.66	0.934(23)	0.88	0.765(58)	1.25
(18,12)	0.5509(54)	0.49	0.924(12)	0.15	0.809(28)	1.00

TABLE VIII. FSHS fit with a correction term. The fit function: $\xi = C_0^H + C_1^H X + C_2^H L m_f^\alpha$. The fitted region is $m_f \geq 0.05$ and $\xi_\pi \geq 8$.

$\alpha = 1$	γ	C_0^H	C_1^H	C_2^H	χ^2/dof
ξ_π	0.791(57)	$-0.004(25)$	1.74(14)	1.12(20)	0.66
ξ_F	0.965(91)	$-0.016(11)$	0.419(44)	0.026(65)	0.74
ξ_ρ	0.80(25)	0.003(190)	2.78(99)	$-0.01(1.30)$	0.73

$\alpha = 2$	γ	C_0^H	C_1^H	C_2^H	χ^2/dof
ξ_π	0.620(12)	$-0.001(25)$	2.421(35)	0.98(21)	0.74
ξ_F	0.941(30)	$-0.016(10)$	0.432(11)	0.030(72)	0.74
ξ_ρ	0.792(83)	0.001(190)	2.80(23)	$-0.1(1.2)$	0.73

omitting the correction term in the ξ_F. The result is summarized in Table IX. This fit works well, and gives a reasonable value of the χ^2/dof. The resulting α is close to unity. A similar value of α is also obtained from a fit without the correction term in the ξ_ρ as shown in Table X. This means that the exponent of the correction term is close

TABLE IX. Simultaneous FSHS fit with a correction term, $\xi = C_0^H + C_1^H X + C_2^H L m_f^\alpha$, where α is free parameter, but $C_2^F = 0$. The fitted region is $m_f \geq 0.05$ and $\xi_\pi \geq 8$. Degrees of freedom are equal to 32.

γ	α	χ^2/dof
0.9292(82)	0.879(53)	0.67

	C_0^H	C_1^H	C_2^H
ξ_π	$-0.004(25)$	1.290(98)	1.538(39)
ξ_F	$-0.015(10)$	0.4366(38)	$\cdots$
ξ_ρ	0.01(19)	2.280(64)	0.61(10)

TABLE X. Simultaneous FSHS fit with a correction term, $\xi = C_0^H + C_1^H X + C_2^H L m_f^\alpha$, where α is free parameter, but $C_2^\rho = 0$. The fitted region is $m_f \geq 0.05$ and $\xi_\pi \geq 8$. Degrees of freedom are equal to 32.

γ	α	χ^2/dof
0.807(18)	0.949(74)	0.77

	C_0^H	C_1^H	C_2^H
ξ_π	$-0.001(25)$	1.65(11)	1.174(66)
ξ_F	$-0.011(10)$	0.516(15)	$-0.107(19)$
ξ_ρ	0.04(18)	2.754(63)	$\cdots$

to unity in our data, while γ's from the two fits are different from each other. The difference is regarded as the ambiguity in this estimate. It is also possible to carry out a simultaneous fit without the corrections in both the ξ_F and ξ_ρ, and fits with the correction terms for all the observables using the fixed $\alpha = 1$ and $\alpha = (3 - 2\gamma)/(1 + \gamma)$, because our data prefer $\alpha \sim 1$ in the above fits. Note that the last one is inspired by the analytic expression of the solution of the Schwinger-Dyson equation [49]. Figure 19 shows the fit result with $\alpha = 1$ as a typical result of the simultaneous fit. These results are shown in Table XI and their γ's agree
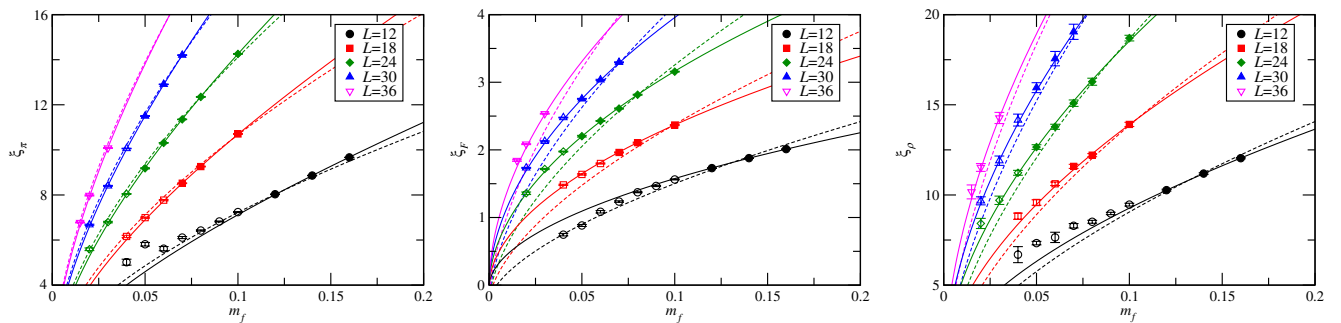

FIG. 19 (color online). Simultaneous FSHS fit in ξ_π (left), ξ_F (center), and ξ_ρ (right) with $\alpha = 1$. The filled symbols are included in the fit, but the open symbols are omitted. The fitted region is $m_f \geq 0.05$ and $\xi_\pi \geq 8$. The solid curve is the fit result. For a comparison, the simultaneous fit result without correction terms is also plotted by the dashed curve, whose $\chi^2/\text{dof} = 83$.

TABLE XI. Simultaneous FSHS fit with a correction term, $\xi = C_0^H + C_1^H X + C_2^H L m_f^\alpha$ using several choices of α. The fitted region is $m_f \geq 0.05$ and $\xi_\pi \geq 8$.

$\alpha = 0.889(55)$	C_0^H	C_1^H	C_2^H
ξ_π	$-0.005(25)$	$1.338(96)$	$1.494(37)$
ξ_F	$-0.0275(98)$	$0.4435(36)$	$\cdots$
ξ_ρ	$0.53(16)$	$2.476(39)$	$\cdots$
$\gamma = 0.9130(76)$, $\chi^2/\text{dof} = 1.73$, $\text{dof} = 33$			
$\alpha = 1$ fixed	C_0^H	C_1^H	C_2^H
ξ_π	$-0.014(24)$	$1.61(10)$	$1.31(15)$
ξ_F	$-0.012(10)$	$0.484(30)$	$-0.068(44)$
ξ_ρ	$0.01(19)$	$2.60(17)$	$0.25(24)$
$\gamma = 0.874(25)$, $\chi^2/\text{dof} = 0.75$, $\text{dof} = 32$			
$\alpha = \frac{3-2\gamma}{1+\gamma}$ fixed	C_0^H	C_1^H	C_2^H
ξ_π	$0.020(24)$	$1.52(39)$	$1.17(35)$
ξ_F	$-0.011(10)$	$0.572(34)$	$-0.158(52)$
ξ_ρ	$0.03(19)$	$2.91(30)$	$-0.15(36)$
$\gamma = 0.775(56)$, $\chi^2/\text{dof} = 0.93$, $\text{dof} = 32$			

within the above ambiguity. Under the assumption that all the observables give a universal γ, we estimate $\gamma = 0.78$–0.93.

It is noted that a simultaneous fit including the lighter mass with $m_f \geq 0.015$ in $\xi_\pi \geq 6.8$ fails with a large $\chi^2/\text{dof} = 3.5$ even if the mass correction is included. This is because the chiral property is dictated by SχSB and should not be consistent with universal hyperscaling near the chiral limit.

To summarize, using the fits with the correction term, we estimated the value of γ from the three observables, and obtain $\gamma = 0.62$–0.97 which depends on the observables and the correction term in the fit form. Furthermore, we carry out simultaneous FSHS fits with the correction term, since a universal γ would be expected if the theory is very close to the conformal phase boundary even in the SχSB phase. The resulting γ in the simultaneous fits reads 0.78–0.93. These estimated γ's would be identified as the mass anomalous dimension in the walking regime.

V. SUMMARY AND DISCUSSION

In search for a candidate for the walking technicolor, we have investigated meson spectrum of $N_f = 8$ QCD by the lattice simulations based on the HISQ action for $\beta = 6/g^2 = 3.8$, and for the fermion bare mass range $m_f = 0.015$–0.16 depending on the volume size $L^3 \times T$ with $(L, T) = (12, 16), (18, 24), (24, 32), (30, 40), (36, 48)$.

We found that the data of F_π, M_π are consistent with the SχSB well described by the ChPT, suggesting that $F \equiv F_\pi(m_f \to 0) \neq 0$, and $M_\pi(m_f \to 0) = 0$, and M_ρ is also nonvanishing $M_\rho(m_f \to 0) \neq 0$ in the chiral limit extrapolation. the ρ mass in units of the π decay constant was

determined and shown in Eq. (26). We further found that the chiral condensate $\langle \bar\psi \psi \rangle$ also has a nonzero value in the chiral limit, which nicely coincides with those from the GMOR relation in that limit. In these analysis we used $0.015 \leq m_f \leq 0.04$.

The salient feature of our collaboration is that we have been investigating $N_f = 4, 8, 12, 16$ on the setting of HISQ action with the same systematics in order to study the N_f dependence of the physics systematically [21,36]. Thus, our analyses for $N_f = 8$ are made in comparison with those for $N_f = 4$ and 12 of our group. The qualitative features of $N_f = 8$ near the chiral limit were found to be similar to those of the $N_f = 4$ case: The $N_f = 4$ data indicated robust signals of the SχSB phase. The result was contrasted with that of the $N_f = 12$ where in the previous study the ChPT analysis was not self-consistent, while the finite-size hyperscaling (FSHS) relation held consistently with the conformal window.

We then checked whether this SχSB phase is close to the conformal window, having some remnant of the infrared conformality. Remarkably enough, in contrast to the data near the chiral limit ($m_f \leq 0.04$) indicating the SχSB, those for the relatively large fermion bare mass $m_f \geq 0.05$ away from the chiral limit actually exhibited a FSHS with the scaling exponent $\gamma(M_\pi) \simeq 0.57$ ($\chi^2/\text{dof} = 2.5$), $\gamma(F_\pi) \simeq 0.93$ ($\chi^2/\text{dof} = 0.7$), $\gamma(M_\rho) \simeq 0.80$ ($\chi^2/\text{dof} = 0.7$). The value of γ is nonuniversal depending on the observable, with χ^2/dof for M_π being large compared to the others. The existence of FSHS is in contrast to our $N_f = 4$ data where we showed no trace of the hyperscaling even for large m_f region and hence no sign of the conformality as in the ordinary QCD. This implies that

there exists a remnant of the infrared conformality where the SχSB effects are negligible (for a schematic view, see case 2 in Fig. 1).

These hyperscaling relations were obtained for relatively large m_f, $m_f \gtrsim 0.05$, in contrast to the FSHS in the conformal window, where FSHS becomes arbitrarily accurate in the chiral limit. Therefore, there could exist large mass corrections on the hyperscaling relation. If we include possible mass corrections on FSHS for each observable, we obtained γ, $0.62 \lesssim \gamma \lesssim 0.97$. Here the χ^2/dof for M_π was improved to the level of the others.

We then performed a simultaneous fit over all the observables based on certain model fitting functions including the mass corrections to see if the universality of γ can be improved by the corrections. To our surprise we found that certain model fitting functions in fact yield a universal value of γ, $0.78 \lesssim \gamma \lesssim 0.93$, with the variations depending on the model fitting function. Since this result is obtained at a single value of β, it is important to see this feature holds in the continuum limit, which will be studied by carrying out simulations with multiple values of β. The possibility of such a large scaling exponent γ was discussed using Dirac eigenmodes in Ref. [34].

The anomalous dimension discussed in the walking technicolor is of course the value in the chiral limit. The lesson from the SD equation analysis in the conformal window tells us [49] that the value of γ obtained by the hyperscaling relation without corrections is an "effective" one which is distorted by the mass corrections. On the other hand, the value determined by the fit explicitly incorporating the mass corrections just corresponds to the γ_* (γ_m at the infrared fixed point) in the chiral limit and hence is of direct relevance to the walking technicolor. Although the γ_m so determined is the value at infrared scale, it coincides with the one discussed in the walking technicolor evaluated at the ultraviolet scale, as far as the infrared conformality for the wide scale hierarchy exists.

Finally, we should comment on the possible light flavor-singlet scalar meson in $N_f = 8$ QCD. The walking technicolor predicts [1,5] a light composite Higgs-like scalar boson, the technidilaton, as a pseudo-NG boson of the approximate scale invariance inherent to the walking dynamics. Actually, it was shown [6] that the technidilaton is consistent with all the current data of the 125 GeV boson discovered at LHC. Then, if the $N_f = 8$ QCD behaves as a walking theory with approximate scale invariance, it would be expected that a light flavor-singlet scalar composite does exist. These studies are currently under way and details will be reported elsewhere. Since the quantum number of such an object is the same as that of the scalar glueballs which may also be light, the lattice analyses near infrared conformality should be done with great care about the possible mixing with each other. As such we made preliminary studies of both flavor-singlet scalar and scalar

glueballs for $N_f = 12$. We found a hint of a flavor-singlet scalar bound state lighter than π for $N_f = 12$ [50].

Summarizing all our analyses we may infer that a typical technicolor ("one-family model") as modeled by the $N_f = 8$ QCD can be a walking technicolor theory having an approximate scale invariance with large anomalous dimension $\gamma_m \sim 1$.

APPENDIX A: DATA TABLES IN THE $N_f = 8$ CASE

The $N_f = 8$ simulations are done at $\beta = 3.8$ with the fixed aspect ratio $L/T = 3/4$: $(L, T) = (12, 16)$, $(18, 24)$, $(30, 40)$, and $(36, 48)$ and with various fermion masses m_f. Resultant values of F_π, M_π, M_{SC}, $M_{\rho(PV)}$, $M_{\rho(VT)}$, and $\langle \bar\psi \psi \rangle$ for each parameter, together with the number of trajectories N_{trj} used for the measurements after thermalzation are summarized in Tables XII, XIII, XIV, XV, and XVI.

APPENDIX B: SIMULATIONS OF $N_f = 4$ QCD

In this Appendix, we show the results of simulations for $N_f = 4$ QCD. We take $\beta = 3.7$, and $(L, T) = (12, 18)$, $(16, 24)$, and $(20, 30)$. For each lattice size, we carry out simulations for various input m_f, and resultant values of F_π, M_π, M_{SC}, and $\langle \bar\psi \psi \rangle$ for each parameter, together with the number of trajectories N_{trj} used for the measurements after thermalization, are summarized in Tables XVII, XVIII, and XIX.

In Fig. 20, we plot M_π^2 (left panel) and F_π as functions of m_f. Curves in each figure are obtained by fitting $c_1 m_f + c_2 m_f^2$ and $c_3 + c_4 m_f + c_5 m_f^2$ to the largest-volume (i.e., $L = 20$, $T = 30$) data of M_π^2 and F_π, respectively. Fit results are $c_1 = 4.36(3)$, $c_2 = 4.3(1.0)$, $c_3 = 0.0873(10)$, $c_4 = 1.846(87)$, and $c_5 = -12.3(1.6)$. These plots show typical behavior of a theory which is in the SχSB phase, namely, M_π^2 is well fitted by a linear function (plus small quadratic correction) of m_f, and F_π clearly has a nonzero value in the chiral limit. As further confirmation, we also plot data of $\langle \bar\psi \psi \rangle$ obtained from the largest-volume

TABLE XII. Results of the spectra on $V = 12^3 \times 16$, with $t_{\min} = 10$.

m_f	N_{trj}	F_π	M_π	M_{SC}	$M_{\rho(\text{PV})}$	$M_{\rho(\text{VT})}$	$\langle \bar\psi \psi \rangle$
0.04	1224	0.0622(15)	0.4181(110)	0.4397(113)	0.5574(370)	0.5389(360)	0.02167(4)
0.05	1284	0.0735(12)	0.4844(65)	0.4987(72)	0.6108(81)	0.6157(71)	0.02704(5)
0.06	1224	0.0904(15)	0.4681(79)	0.4664(120)	0.6372(237)	0.6343(218)	0.03269(6)
0.07	1264	0.1030(9)	0.5091(38)	0.5168(64)	0.6910(102)	0.6882(87)	0.03802(7)
0.08	1264	0.1144(6)	0.5352(23)	0.5439(26)	0.7093(69)	0.7031(53)	0.04328(6)
0.09	1300	0.1222(7)	0.5686(17)	0.5774(24)	0.7478(54)	0.7449(54)	0.04826(7)
0.10	1300	0.1302(6)	0.6033(19)	0.6116(23)	0.7886(65)	0.7866(61)	0.05319(6)
0.12	2500	0.1442(4)	0.6694(12)	0.6760(13)	0.8556(43)	0.8517(43)	0.06265(4)
0.14	2600	0.1565(3)	0.7384(11)	0.7460(13)	0.9321(38)	0.9317(39)	0.07181(4)
0.16	3524	0.1676(2)	0.8056(8)	0.8142(9)	1.0032(29)	1.0029(26)	0.08059(3)

TABLE XIII. Results of the spectra on $V = 18^3 \times 24$ with $t_{\text{results}} = 16$.

m_f	N_{trj}	F_π	M_π	M_{SC}	$M_{\rho(\text{PV})}$	$M_{\rho(\text{VT})}$	$\langle \bar\psi \psi \rangle$
0.04	712	0.0823(5)	0.3421(29)	0.3445(33)	0.4901(96)	0.4842(107)	0.02295(3)
0.05	752	0.0910(6)	0.3886(15)	0.3908(19)	0.5323(84)	0.5248(79)	0.02818(3)
0.06	904	0.0999(5)	0.4317(15)	0.4351(17)	0.5900(63)	0.5943(52)	0.03334(2)
0.07	1064	0.1090(5)	0.4734(10)	0.4777(13)	0.6436(63)	0.6398(64)	0.03849(3)
0.08	844	0.1170(5)	0.5144(10)	0.5181(12)	0.6782(49)	0.6776(56)	0.04354(4)
0.10	876	0.1315(4)	0.5948(11)	0.5993(12)	0.7729(65)	0.7698(56)	0.05334(3)

TABLE XIV. Results of the spectra on $V = 24^3 \times 32$ with $t_{\min} = 22$.

m_f	N_{trj}	F_π	M_π	M_{SC}	$M_{\rho(\text{PV})}$	$M_{\rho(\text{VT})}$	$\langle \bar\psi \psi \rangle$
0.02	744	0.0566(8)	0.2330(25)	0.2367(37)	0.3508(117)	0.3461(111)	0.01188(3)
0.03	728	0.0715(4)	0.2832(14)	0.2851(14)	0.4044(96)	0.4018(101)	0.01746(2)
0.04	864	0.0823(2)	0.3353(7)	0.3382(7)	0.4678(57)	0.4693(57)	0.02290(1)
0.05	752	0.0918(5)	0.3826(10)	0.3851(11)	0.5274(54)	0.5228(53)	0.02825(2)
0.06	1848	0.1012(3)	0.4295(6)	0.4327(6)	0.5742(58)	0.5826(55)	0.03345(2)
0.07	864	0.1088(3)	0.4731(6)	0.4767(7)	0.6288(74)	0.6345(75)	0.03853(1)
0.08	816	0.1173(3)	0.5145(8)	0.5187(8)	0.6783(81)	0.6795(71)	0.04357(2)
0.10	948	0.1315(3)	0.5940(5)	0.5987(6)	0.7790(65)	0.7760(68)	0.05334(1)

TABLE XV. Results of the spectra on $V = 30^3 \times 40$ with $t_{\min} = 28$.

m_f	N_{trj}	F_π	M_π	M_{SC}	$M_{\rho(\text{PV})}$	$M_{\rho(\text{VT})}$	$\langle \bar\psi \psi \rangle$
0.02	996	0.0578(2)	0.2227(9)	0.2245(10)	0.3225(75)	0.3221(65)	0.01189(1)
0.03	1044	0.0709(3)	0.2801(7)	0.2818(8)	0.3967(87)	0.3940(69)	0.01744(1)
0.04	1060	0.0826(2)	0.3354(4)	0.3377(4)	0.4718(110)	0.4730(99)	0.02294(1)
0.05	1108	0.0918(2)	0.3834(5)	0.3859(5)	0.5317(92)	0.5302(80)	0.02822(1)
0.06	788	0.1012(3)	0.4304(4)	0.4332(4)	0.5853(132)	0.5887(123)	0.03344(1)
0.07	732	0.1098(2)	0.4735(4)	0.4769(4)	0.6349(141)	0.6329(120)	0.03855(1)

TABLE XVI. Results of the spectra on $V = 36^3 \times 48$ with $t_{\min} = 32$.

m_f	N_{trj}	F_π	M_π	M_{SC}	$M_{\rho(\text{PV})}$	$M_{\rho(\text{VT})}$	$\langle \bar\psi \psi \rangle$
0.015	1004	0.0512(3)	0.1883(5)	0.1900(7)	0.2825(107)	0.2904(71)	0.00906(1)
0.02	808	0.0579(2)	0.2216(7)	0.2229(8)	0.3202(60)	0.3232(61)	0.01189(1)
0.03	996	0.0704(2)	0.2801(5)	0.2818(6)	0.3964(86)	0.3935(71)	0.01745(1)

TABLE XVII.   Results of the spectra for $N_f = 4$ on $V = 12^3 \times 18$.

m_f	N_{trj}	F_π	M_π	M_{SC}	$\langle \bar\psi \psi \rangle$
0.01	500	0.0858(22)	0.2373(30)	0.3022(79)	0.01471(48)
0.02	500	0.1141(11)	0.3016(26)	0.3502(52)	0.02332(28)
0.03	500	0.12900(69)	0.3706(11)	0.4087(28)	0.03056(15)
0.04	500	0.13842(67)	0.4283(14)	0.4705(21)	0.03683(16)
0.05	500	0.14893(59)	0.4778(10)	0.5173(27)	0.04291(29)

TABLE XVIII.   Results of the spectra for $N_f = 4$ on $V = 16^3 \times 24$.

m_f	N_{trj}	F_π	M_π	M_{SC}	$\langle \bar\psi \psi \rangle$
0.005	500	0.08195(76)	0.16356(87)	0.2235(65)	0.01102(21)
0.01	500	0.10258(78)	0.21390(75)	0.2763(27)	0.016413(8)
0.02	500	0.11980(71)	0.2996(11)	0.3484(16)	0.02415(12)
0.03	500	0.13059(59)	0.36739(75)	0.4099(20)	0.03060(11)
0.04	500	0.14124(31)	0.42524(60)	0.4659(11)	0.03697(11)

TABLE XIX.   Results of the spectra for $N_f = 4$ on $V = 20^3 \times 30$.

m_f	N_{trj}	F_π	M_π	M_{SC}	$\langle \bar\psi \psi \rangle$
0.01	180	0.10443(40)	0.20966(68)	0.2611(29)	0.01637(5)
0.02	380	0.11955(31)	0.29873(83)	0.3413(12)	0.02396(5)
0.03	350	0.13144(33)	0.36699(89)	0.4082(13)	0.030789(36)
0.04	200	0.14160(24)	0.42579(86)	0.4663(13)	0.037317(39)

simulation as a function of m_f in Fig. 21. In the figure, we also plotted $F_\pi^2 M_\pi^2/(4m_f)$ ($\equiv \Sigma$) which are calculated from the data of M_π and F_π at each m_f. Curves in the figure are the results of quadratic fits, and resultant values in the chiral limit are 0.00845(14) and 0.00832(21) for $\langle \bar\psi \psi \rangle$ and Σ, respectively.

To estimate the amount of systematic error of chiral extrapolation, we did the same analysis that was done in Sec. III D. In Fig. 22, we show the result of ChPT

extrapolation which is matched to the quadratic fit result at $m_f = 0.01$, the smallest mass we simulate. The value of F_π in the chiral limit (F) obtained by this procedure is $F = 0.0730$, while the quadratic fit gives $F = 0.0873(10)$. We should note here that there is no visible chiral-log behavior in our data in the range of $0.01 \leq m_f \leq 0.04$, therefore the estimate of the amount of chiral-log effect in the chiral limit given here should be understood as the maximum possible. We should also mention here the values of chiral
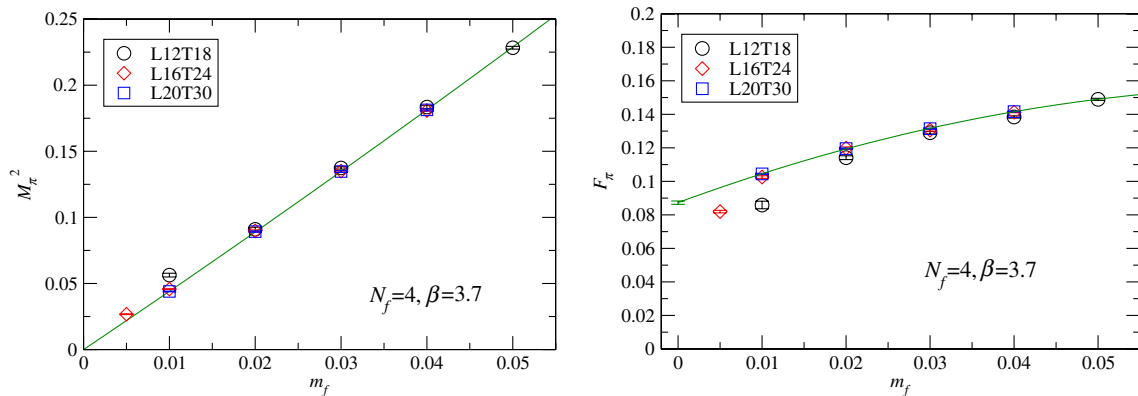

FIG. 20 (color online). M_π^2 (left panel) and F_π as functions of m_f for $N_f = 4$ QCD with $\beta = 3.7$. Curves in each figure are obtained by fitting $c_1 m_f + c_2 m_f^2$ and $c_3 + c_4 m_f + c_5 m_f^2$ to the largest-volume data of M_π^2 and F_π, respectively.
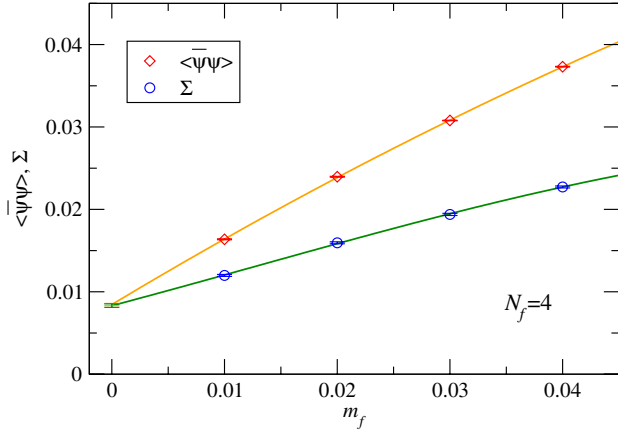
FIG. 21 (color online). $\langle \bar{\psi}\psi \rangle$ as a function of m_f for $N_f = 4$ QCD with $\beta = 3.7$, $L = 20$, $T = 30$. The data points indicated by Σ are calculated through $F_\pi^2 M_\pi^2/(4m_f)$ with the data of M_π and F_π at each m_f. Curves in the figure are the results of quadratic fits.
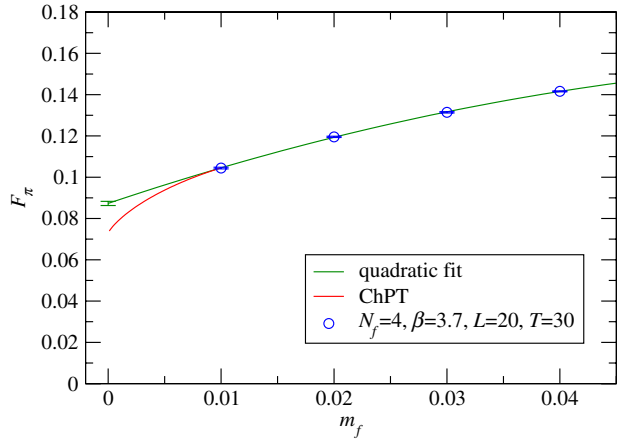

FIG. 22 (color online). Quadratic fit to the largest volume data of F_π and ChPT extrapolation. The value in the chiral limit by ChPT is $F_\pi = 0.0730$, while the quadratic fit gives $F_\pi = 0.0873(10)$.
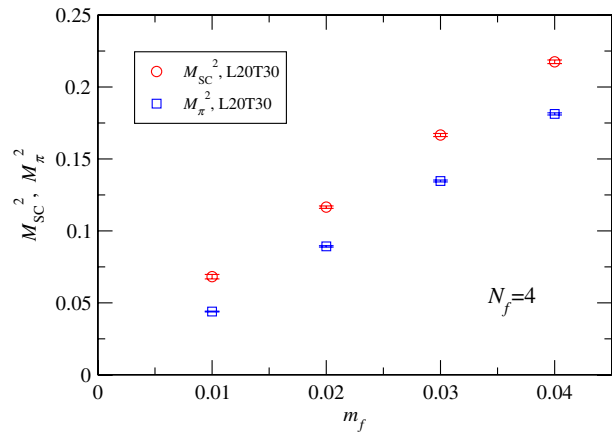
FIG. 23 (color online). Comparison of M_{SC}^2 and M_π^2 as a function of m_f for $N_f = 4$ QCD with $\beta = 3.7$.

expansion parameter X. By using $F = 0.0873$, the expansion parameter at $m_f^{\min} = 0.01$ is estimated as $X \simeq 0.3$ while the one at $m_f^{\max} = 0.04$ is $X \simeq 1.2$. This confirms the consistency of using ChPT analysis and thus, we conclude that $N_f = 4$ QCD is in the SχSB phase.

In Fig. 23, we plot the values of M_{SC}^2 together with values of M_π^2 for each m_f. This comparison shows the amount of flavor-symmetry-breaking effect in our simulation for $N_f = 4$ QCD with $\beta = 3.7$.

Finally, we show the finite-size hyperscaling test for $N_f = 4$ QCD by using the data of F_π obtained here. In Fig. 24, we show the finite-size hyperscaling plot for input values of $\gamma = 0.0$, 1.0, and 2.0. As we expect, the data show no alignment in the range of $0 \leq \gamma \leq 2$. This should be regarded as a typical property of QCD-like theory, and contrasted to the case of $N_f = 8$.

APPENDIX C: ESTIMATE OF CHIRAL LOG CORRECTIONS

In this Appendix we estimate the effect of the chiral log correction for the F and $\langle \bar{\psi}\psi \rangle$ in the chiral limit. Since both the NLO ChPT formulas Eqs. (21) and (22) contain the B and F, to match the polynomial fit to the NLO ChPT formula at the matching point m_f^c, we need to solve the matching conditions using Eqs. (21) and (22), and their derivatives at m_f^c, simultaneously. The m_f^c dependence for the B and F are plotted in Fig. 25. For comparison the polynomial fit results are shown by the dashed lines. The value of the X in Eq. (15) evaluated using the obtained F at each m_f^c is presented in Fig. 26. A reasonable value of $X \sim 1$ is obtained only in the much smaller m_f region than the m_f used in our simulation. At $m_f^c = 0.00199$, we obtain $X = 1$ and $F = 0.207$.

To study the chiral log correction on the chiral condensate, the value in the chiral limit is also estimated from the B and F at each m_f^c using the GMOR relation, $\langle \bar{\psi}\psi \rangle|_{m_f \to 0} = BF^2/2$ presented in Fig. 27. When one chooses the matching point where $X = 1$, one obtains roughly a half value of the polynomial fit result of the direct measurement.

Similar results are obtained from different analyses, such as using the expansion parameter $2M_\pi^2/(4\pi F_\pi)^2$ instead of x in the NLO formulas Eqs. (21) and (22), or using $\langle \bar{\psi}\psi \rangle$ instead of M_π^2/m_f or F_π for matching. Therefore we use only the result in the first case to estimate the chiral log corrections in Sec. III D.

APPENDIX D: $P(\gamma)$ ANALYSIS

In this Appendix in order to perform the analysis that does not assume the functional form of fitting in FSHS, we consider $P(\gamma)$ defined in Ref. [21].

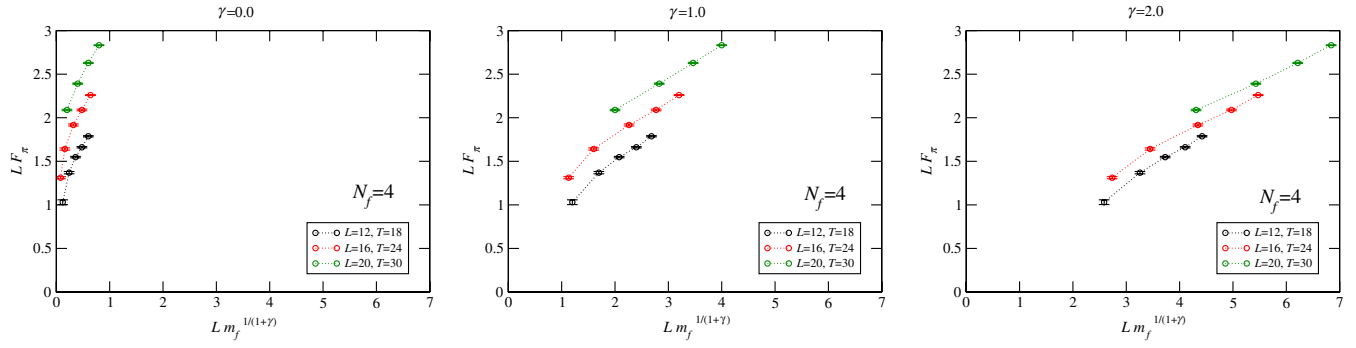To quantify the ''alignment'' we introduce an evaluation function $P(\gamma)$ for an observable p as follows. Suppose ξ^j is

FIG. 24 (color online).   Finite size hyperscaling test of F_π in $N_f = 4$ QCD. Input values of γ are, from left to right panels, $\gamma = 0.0$, 1.0, and 2.0, respectively.
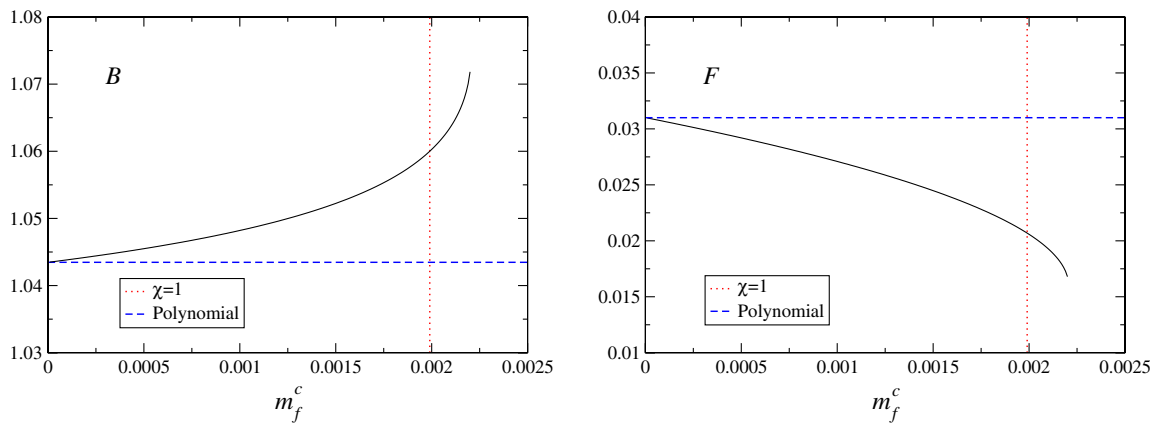

FIG. 25 (color online).   Low energy constants B (left) and F (right) estimated by matching NLO ChPT formulas at the matching point m_f^c. The dashed and dotted lines denote the polynomial fit result and m_f^c at $\mathcal{X} = 1$, respectively.
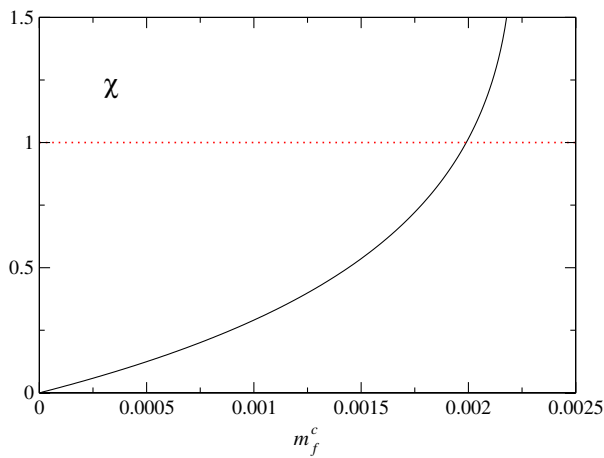

FIG. 26 (color online). $\mathcal{X}$ estimated by matching NLO ChPT formulas at the matching point m_f^c. The dotted line denotes $\mathcal{X} = 1$.
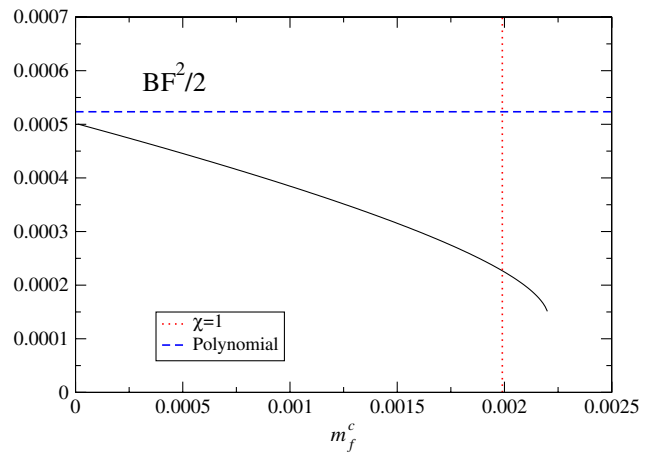

FIG. 27 (color online). $\Sigma|_{m_f \to 0}$ estimated by matching NLO ChPT formulas at the matching point m_f^c. The dashed and dotted lines denote the polynomial fit result and m_f^c at $\mathcal{X} = 1$, respectively.
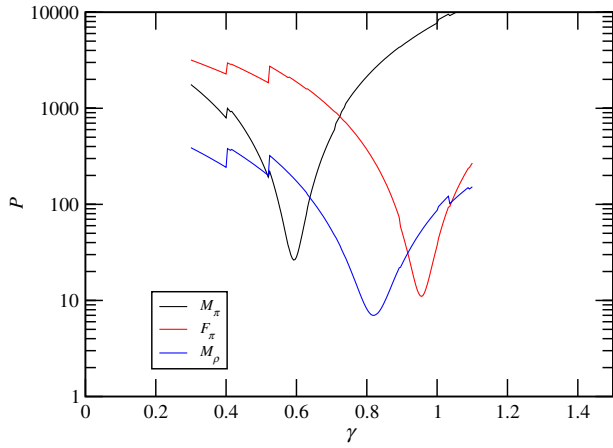
FIG. 28 (color online). $P(\gamma)$ in M_π F_π, and M_ρ in $N_f = 8$ QCD.

TABLE XX. Optimal γ to make $P(\gamma)$ minimum with statistical error.

	M_π	F_π	M_ρ
γ	0.593(2)	0.955(4)	0.820(20)

interpolation of the data points of the fixed lattice size L for simplicity, which should be a good approximation of ξ for large x.

This evaluation function takes a smaller value when the data points are more closely collapsed to the line $f^{(K_L)}$ and thus provides a measure of the alignment. $P(\gamma)$ varies as the choice of parameter γ and should show a minimum at a certain value of γ when the optimal alignment of data is achieved. We take it as the optimal value of γ.

We then estimate the uncertainty of the optimal γ by properly taking account of the statistical fluctuation of ξ_i as well as its effect to the line $f^{(K_L)}$. For this purpose, we employ the parametric bootstrap method, in which the data point is simulated by a random sample generated by Gaussian distribution with the mean ξ^j and the standard deviation $\delta\xi^j$. The distribution of γ is thus obtained for a large number of these samples, from which the variance of γ is estimated. The systematic error associated with the interpolation will be estimated by choosing different functional form with linear or quadratic splines as will be discussed subsequently.

We use the data as the overlapped region sandwiched between $m_f = 0.015$ on $L = 36$ and $m_f = 0.03$ on $L = 36$. Figure 28 is the result of $P(\gamma)$ for all M_π, F_π, and M_ρ and there are minima of $P(\gamma)$. The γ value at the minimum of $P(\gamma)$ is written on Table XX.

a data point of the measured observable p at $x_j = L_j \cdot m_j^{1/(1+\gamma)}$ and $\delta\xi^j$ is the error of ξ^j. j labels distinction of parameters L and m_f. Let K be a subset of data points $\{(x_k, \xi_k)\}$ from which we construct a function $f^{(K)}(x)$ which represents the subset of data. Then, the evaluation function is defined as

$$P(\gamma) = \frac{1}{\mathcal{N}} \sum_L \sum_{j \notin K_L} \frac{|\xi^j - f^{(K_L)}(x_j)|^2}{|\delta\xi^j|^2}, \qquad \text{(D1)}$$

where L runs through all the lattice sizes we have, the sum over j is taken for a set of data points which do not belong to K_L which includes all the data obtained on the lattice with size L. $\mathcal{N}$ denotes the total number of summation. Here, we choose for the function $f^{(K_L)}$ a linear

[1] K. Yamawaki, M. Bando, and K.-i. Matumoto, Phys. Rev. Lett. **56**, 1335 (1986).
[2] Similar works without notion of anomalous dimension and scale symmetry were done: B. Holdom, Phys. Lett. **150B**, 301 (1985); T. Akiba and T. Yanagida, *ibid.* **169B**, 432 (1986); T. W. Appelquist, D. Karabali, and L. Wijewardhana, Phys. Rev. Lett. **57**, 957 (1986).
[3] T. Maskawa and H. Nakajima, Prog. Theor. Phys. **52**, 1326 (1974); **54**, 860 (1975); R. Fukuda and T. Kugo, Nucl. Phys. **B117**, 250 (1976).
[4] V. Miransky, Nuovo Cimento Soc. Ital. Fis. A **90**, 149 (1985).
[5] M. Bando, K.-i. Matumoto, and K. Yamawaki, Phys. Lett. B **178**, 308 (1986).
[6] S. Matsuzaki and K. Yamawaki, Phys. Lett. B **719**, 378 (2013); **86**, 115004 (2012), and references therein.
[7] W. E. Caswell, Phys. Rev. Lett. **33**, 244 (1974); T. Banks and A. Zaks, Nucl. Phys. **B196**, 189 (1982).

[8] T. Appelquist, J. Terning, and L. C. R. Wijewardhana, Phys. Rev. Lett. **77**, 1214 (1996).
[9] V. A. Miransky and K. Yamawaki, Phys. Rev. D **55**, 5051 (1997).
[10] Y. Iwasaki, K. Kanaya, S. Sakai, and T. Yoshie, Phys. Rev. Lett. **69**, 21 (1992).
[11] Y. Iwasaki, K. Kanaya, S. Kaya, S. Sakai, and T. Yoshie, Phys. Rev. D **69**, 014507 (2004).
[12] F. R. Brown, H. Chen, N. H. Christ, Z. Dong, R. D. Mawhinney, W. Schaffer, and A. Vaccarino, Phys. Rev. D **46**, 5655 (1992).
[13] P. Damgaard, U. M. Heller, A. Krasnitz, and P. Olesen, Phys. Lett. B **400**, 169 (1997).
[14] See, for example, J. Giedt, Proc. Sci., LATTICE2012 (2012) 006; E. T. Neil, Proc. Sci., LATTICE2011 (2011) 009.
[15] T. Appelquist, G. T. Fleming, and E. T. Neil, Phys. Rev. Lett. **100**, 171607 (2008); Phys. Rev. D **79**, 076010 (2009).

[16] A. Deuzeman, M. P. Lombardo, and E. Pallante, Phys. Rev. D **82**, 074503 (2010).

[17] A. Hasenfratz, Phys. Rev. D **82**, 014506 (2010); Phys. Rev. Lett. **108**, 061601 (2012).

[18] T. DeGrand, Phys. Rev. D **84**, 116901 (2011).

[19] K. Ogawa, T. Aoyama, H. Ikeda, E. Itou, M. Kurachi, C.-J. Lin, H. Matsufuru, H. Ohki, T. Onogi, E. Shintani, and T. Yamazaki, Proc. Sci., LATTICE2011 (2011) 081.

[20] C.-J. D. Lin, K. Ogawa, H. Ohki, and E. Shintani, J. High Energy Phys. 08 (2012) 096.

[21] Y. Aoki, T. Aoyama, M. Kurachi, T. Maskawa, K.-i. Nagai, H. Ohki, A. Shibata, K. Yamawaki, and T. Yamazaki (LatKMI Collaboration), Phys. Rev. D **86**, 054506 (2012); Proc. Sci., LATTICE2011 (2011) 053; LATTICE2012 (2012) 029.

[22] E. Itou, arXiv:1212.1353.

[23] Y. Iwasaki, arXiv:1212.4343.

[24] K.-I. Ishikawa, Y. Iwasaki, Y. Nakayama, and T. Yoshie, arXiv:1301.4785 [Phys. Rev. D (to be published)].

[25] Z. Fodor, K. Holland, J. Kuti, D. Nógrádi, and C. Schroeder, Phys. Lett. B **681**, 353 (2009).

[26] X.-Y. Jin and R. D. Mawhinney, Proc. Sci., LATTICE2010 (2010) 055.

[27] M. Hayakawa, K.-I. Ishikawa, Y. Osaki, S. Takeda, S. Uno, and N. Yamada, Phys. Rev. D **83**, 074509 (2011).

[28] See for a review: E. Farhi and L. Susskind, Phys. Rep. **74**, 277 (1981).

[29] E. Farhi and L. Susskind, Phys. Rev. D **20**, 3404 (1979).

[30] S. Matsuzaki and K. Yamawaki, Phys. Rev. D **85**, 095020 (2012).

[31] A. Deuzeman, M. P. Lombardo, and E. Pallante, Phys. Lett. B **670**, 41 (2008).

[32] K. Miura and M. P. Lombardo, Nucl. Phys. **B871**, 52 (2013).

[33] G. Petropoulos, A. Cheng, A. Hasenfratz, and D. Schaich, Proc. Sci., LATTICE2012 (2012) 051.

[34] A. Cheng, A. Hasenfratz, G. Petropoulos, and D. Schaich, arXiv:1301.1355.

[35] E. Follana, Q. Mason, C. Davies, K. Hornbostel, G. P. Lepage, J. Shigemitsu, H. Trottier, and K. Wong (HPQCD and UKQCD Collaboration), Phys. Rev. D **75**, 054502 (2007); A. Bazavov *et al.* (MILC Collaboration), Phys. Rev. D **82**, 074501 (2010).

[36] Y. Aoki, T. Aoyama, M. Kurachi, T. Maskawa, K.-i. Nagai, H. Ohki, A. Shibata, K. Yamawaki, and T. Yamazaki (LatKMI Collaboration), Proc. Sci., LATTICE2011 (2011) 080; LATTICE2012 (2012) 035.

[37] J. Gasser and H. Leutwyler, Ann. Phys. (N.Y.) **158**, 142 (1984); **250**, 465 (1985).

[38] T. DeGrand, Phys. Rev. D **80**, 114507 (2009).

[39] L. Del Debbio and R. Zwicky, Phys. Rev. D **82**, 014502 (2010).

[40] L. Del Debbio, B. Lucini, A. Patella, C. Pica, and A. Rago, Phys. Rev. D **82**, 014509 (2010).

[41] L. Del Debbio, B. Lucini, A. Patella, C. Pica, and A. Rago, Phys. Rev. D **82**, 014510 (2010).

[42] A. Bazavov *et al.*, Phys. Rev. D **85**, 054503 (2012).

[43] See http://physics.indiana.edu/~sg/milc.html.

[44] M. Hasenbusch, Phys. Lett. B **519**, 177 (2001).

[45] K. Bowler, C. Chalmers, R. Kenway, G. Pawley, and D. Roweth, Nucl. Phys. **B284**, 299 (1987).

[46] T. Blum, P. Chen, N. Christ, C. Cristian, C. Dawson, G. Fleming, R. Mawhinney, S. Ohta, G. Siegert, A. Soni, P. Vranas, M. Wingate, L. Wu, and Y. Zhestkov (RBC Collaboration), Phys. Rev. D **68**, 114506 (2003).

[47] V. A. Miransky, Phys. Rev. D **59**, 105003 (1999).

[48] M. Soldate and R. Sundrum, Nucl. Phys. **B340**, 1 (1990); R. S. Chivukula, M. J. Dugan, and M. Golden, Phys. Rev. D **47**, 2930 (1993); M. Harada and K. Yamawaki, Phys. Rep. **381**, 1 (2003).

[49] Y. Aoki, T. Aoyama, M. Kurachi, T. Maskawa, K.-i. Nagai, H. Ohki, A. Shibata, K. Yamawaki, and T. Yamazaki (LatKMI Collaboration), Phys. Rev. D **85**, 074502 (2012).

[50] Y. Aoki, T. Aoyama, M. Kurachi, T. Maskawa, K.-i. Nagai, H. Ohki, E. Rinaldi, A. Shibata, K. Yamawaki, and T. Yamazaki (LatKMI Collaboration), arXiv:1302.4577.